

# SOLSTICE: An Electronic Journal of Geography and Mathematics

Persistent URL:

<http://deepblue.lib.umich.edu/handle/2027.42/58219>

Cite articles as:

Author names(s), Year. Title of article, *Solstice: An Electronic Journal of Geography and Mathematics*, Vol. XX, No. YY. Ann Arbor: Institute of Mathematical Geography.



Deep Blue



IMaGe Home



Solstice Home

Institute of Mathematical Geography, All rights reserved in all formats.  
Works best with a high speed internet connection.

Final version of IMAge logo created by Allen K. Philbrick from original artwork from the Founder.

## VOLUME XXIII, NUMBER 2; December, 2012

### Articles and Notes

Click on the sun/cloud button to see a word cloud of the adjacent article or related material!

On Mathematics of Navigational Calculations for Meridian Sailing



Serdjo Kos  
and  
Tibor K. Pogany



**Part 2. Geosocial Networking:  
A Case from Ann Arbor, Michigan**

David E. Arlinghaus  
and  
Sandra L. Arlinghaus



**A Short Note**

Waldo Tobler

Click on the sun/cloud to see wind maps as an idea of what is to come in people movement maps.



**Update on Varroa Mite Spread**

Diana Sammataro

Click on the sun/cloud to see an associated abstract published elsewhere.



**QR Code Transformations**

Sandra L. Arlinghaus



Institute

Institute

Institute

Institute of Mat

Institute of Mat

Institute of Mat

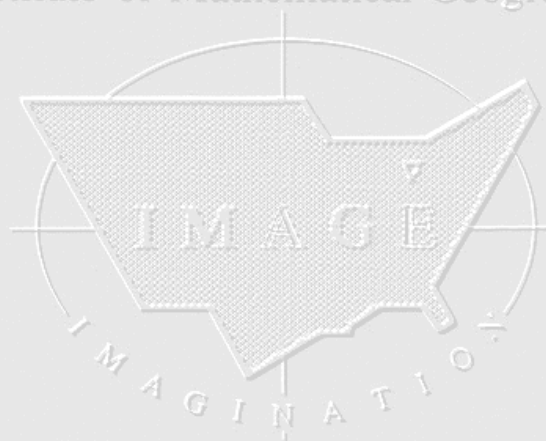
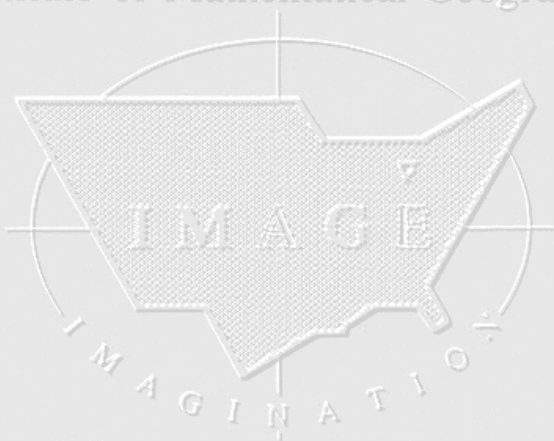


**QR Code Alterations**

Sandra L. Arlinghaus



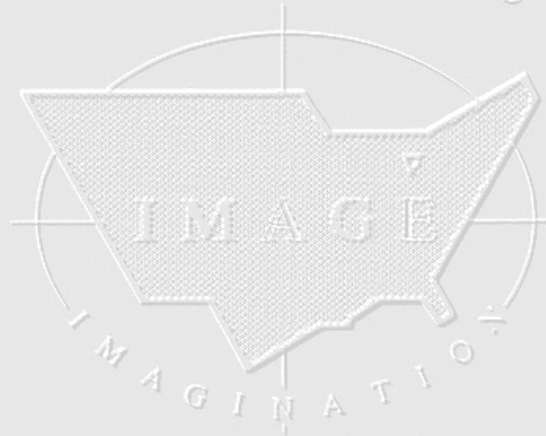
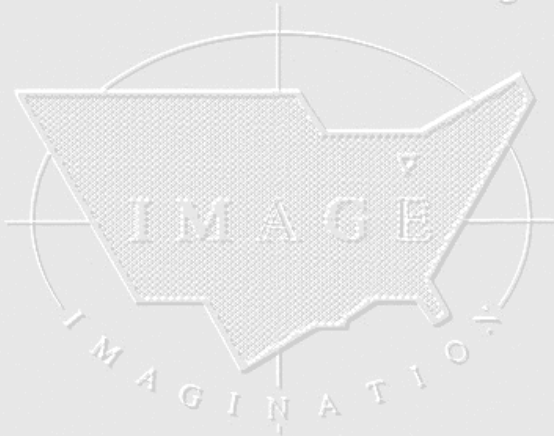
**SOLSTICE MAIL--click on the scrolling marquee to see it. From: William C. Arlinghaus, David Gitterman, Karen Hart, Jo**



Institute of Mathematical Geography

Institute of Mathematical Geography

Institute of Mat



Institute of Mathematical Geography

Institute of Mathematical Geography

Institute of Mat





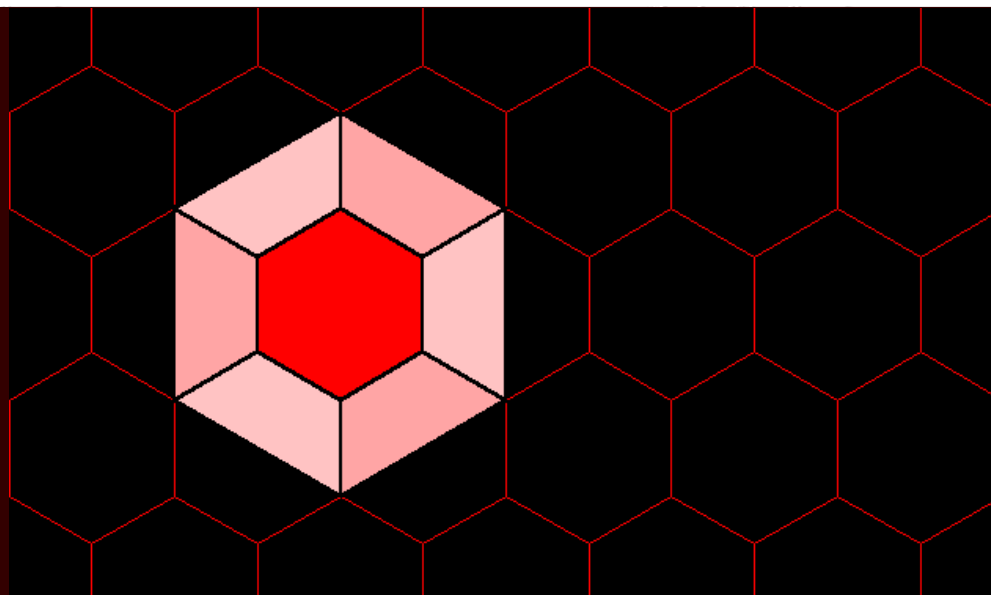
Institute of Mathe



Institute of Mathe



Institute of Mathe



### 1. ARCHIVE

### 2. Editorial Board, Advice to Authors, Mission Statement

### 3. Awards

1.



2.



3.



### RECENT NEWS, 2012

1. *Spatial Mathematics: Theory and Practice Through Mapping*. Sandra L. Arlinghaus and Joseph Kerski, forthcoming (2013), CRC Press. [Linked video](#).
2. The work above is the first volume in a series of books to be published by CRC Press in its series "**Cartography, GIS, and Spatial Science: Theory and Practice.**" If you have an idea for a book to include, or wish to participate in some other way, please contact the series Editor, Sandra L. Arlinghaus.
3. [Virtual Cemetery](#) with William E. Arlinghaus; an ongoing project that continues in development run in the virtual world in parallel with the trust-funded model of a real-world cemetery.

Institute of Mathe



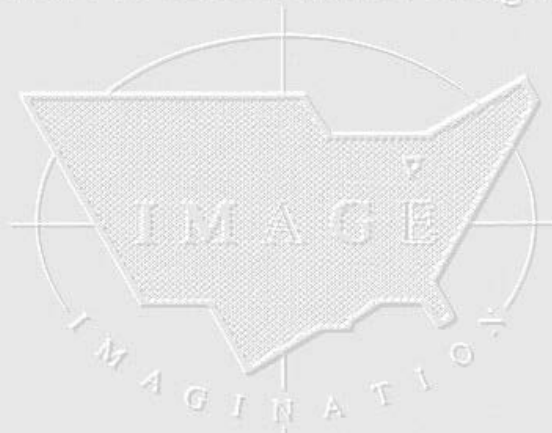
Institute of Mathe



Institute of Mathe



Institute of Mathematical Geography



***Solstice: An Electronic Journal of Geography and Mathematics,***  
**Institute of Mathematical Geography (IMaGe).**  
All rights reserved worldwide, by IMaGe and by the authors.  
Please contact an appropriate party concerning citation of this article:  
[sarhaus@umich.edu](mailto:sarhaus@umich.edu)  
<http://www.imagenet.org>  
<http://deepblue.lib.umich.edu/handle/2027.42/58219>

*Solstice* was a **Pirelli** INTERNETional Award Semi-Finalist, 2001 (top 80 out of over 1000 entries worldwide)

One article in *Solstice* was a **Pirelli** INTERNETional Award Semi-Finalist, 2003 (Spatial Synthesis Sampler).

*Solstice* is listed in the **Directory of Open Access Journals** maintained by the University of Lund where it is maintained as a "searchable" journal.

*Solstice* is listed on the journals section of the website of the American Mathematical Society, <http://www.ams.org/>

*Solstice* is listed in ***Geoscience e-Journals***

IMaGe is listed on the website of the Numerical Cartography Lab of The Ohio State University: [http://ncl.sbs.ohio-state.edu/4\\_homes.html](http://ncl.sbs.ohio-state.edu/4_homes.html)

Congratulations to all *Solstice* contributors.

Remembering those who are gone now but who contributed in various ways to *Solstice* or to IMAge projects, directly or indirectly, during the first 25 years of IMAge:

Allen K. Philbrick | Donald F. Lach | Frank Harary | William D. Drake |  
H. S. M. Coxeter | Saunders Mac Lane | Chauncy D. Harris | Norton S.  
Ginsburg | Sylvia L. Thrupp | Arthur L. Loeb | George Kish |

1964 Boulder Drive,  
Ann Arbor, MI 48104  
734.975.0246

<http://deepblue.lib.umich.edu/handle/2027.42/58219>  
[sarhaus@umich.edu](mailto:sarhaus@umich.edu)

# On the Mathematics of Navigational Calculations for Meridian Sailing

Serdjo Kos and Tibor K. Pogány

*Faculty of Maritime Studies, University of Rijeka, Croatia*

Email: skos@pfri.hr; poganj@pfri.hr

**Abstract.** Meridian sailing is actually a special case of sailing uniquely determined by relative coordinates  $\Delta\varphi, \Delta\lambda$ . In this note we discuss explicit finding of certain navigational parameters. These include loxodrome distance, rhumb line and geographic and geocentric latitude of a position on the globe surface. The latter is expressed in terms of the inverse incomplete elliptic integral of the third kind  $\Pi$ ; we discuss and survey certain traditional and recent methods of computation of this function.

**Key Words:** Meridian (Loxodrome) sailing, Incomplete elliptic integral of the third kind, Numerical quadrature, Binomial series expansion of the integrand, Bulirsch method, Carlson's duplication, Fukushima's  $J$ -method.

## 1. INTRODUCTION

From the nautical point of view, in surface navigation we have two basic ship tracking models when the trajectory is prescribed.

- The first is constant course navigation (or loxodromic navigation), when no course changes occur in a unit of time. Under this assumption we recognize two specific cases:
  - (i) the course line is a meridian (meridian sailing) and
  - (ii) the course line is a parallel or coincides with the equator.
- The second is navigation with a variable rhumb. When the course line cuts meridians pointwise at variable angles, the model is called orthodromic sailing.

We will focus here on loxodromic navigation and its specific case (i). However, because the distance between two parallel lines is the same, regardless of the meridian along which it is measured, the distance  $L_m$  along any meridian between two parallels becomes a constant multiple  $L_{lox} = \sec \alpha \cdot L_m$  of the secant of the constant angle  $\alpha$  between the rhumb line and a meridian on the globe and the meridian distance  $L_m$ . Obviously, it is enough to study meridian sailing's length.

Loxodromic navigation is set by a couple of relative coordinates

$$(\Delta\varphi, \Delta\lambda) = (\varphi_2 - \varphi_1, \lambda_2 - \lambda_1),$$

where  $\varphi_1, \varphi_2$ , and  $\lambda_1, \lambda_2$  stand for the absolute geographic coordinates of latitude and longitude respectively and index 1 denotes the departure, and 2 the arrival positions. The meridian sailing corresponds by definition to  $\Delta\lambda = 0$ , while the sign of  $\Delta\varphi$  determines the general loxodromic course, which is  $K_L = 0^\circ$  for positive, and  $K_L = 180^\circ$  for negative  $\Delta\varphi$ .



In this article we study the meridian (loxodromic) arc length on a meridian on the globe spheroid surface starting at latitude  $\varphi_1$  and finishing at latitude  $\varphi_2$ . Without loss of generality we shall assume that  $\varphi_1 = 0$ , that is  $\Delta\varphi = \varphi_2 \equiv \varphi$  can be taken, i.e. the navigation begins precisely on the equator. Indeed, we have  $\Delta\varphi = (\varphi_2 - \psi) - (\varphi_1 - \psi)$ ,  $\psi$  arbitrary, which reduces the meridian arc length calculation to the case  $\varphi_1 \equiv 0$ .

## 2. MERIDIAN SAILING ON THE ELLIPSOID OF REVOLUTION

Figure 1 presents the ellipsoid of revolution (two-axis or rotational ellipsoid) model of the globe with the equatorial radius  $a$  and polar radius  $b$ . The great ellipse is a planar cross-section of the ellipsoid and the plane containing the symmetry axis. (The associated numerical eccentricity we denote by the usual  $e^2 = 1 - b^2/a^2 \leq 1$ ). On the other hand  $\theta$  signifies the geocentric latitude of the same position  $P$ . Let us mention that  $\tan \theta = (1 - e^2) \tan \varphi$ .

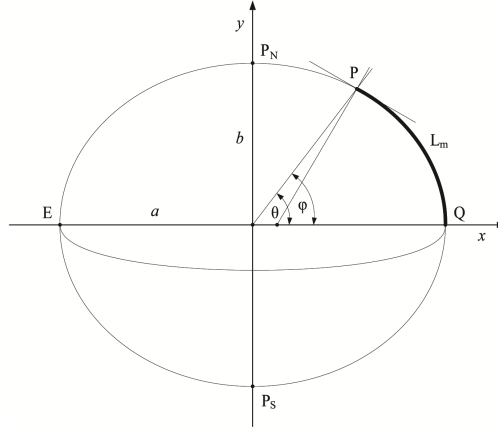


Figure 1. Meridian Ellipse on the Ellipsoid of Revolution.

The meridian ellipse arc length  $L_m$  characterizes the path between departure position  $Q$  at the equator and the arrival position  $P$  and reads as follows

$$L_m = a(1 - e^2) \int_0^\varphi \frac{dt}{(1 - e^2 \sin^2 t)^{3/2}} = \frac{b^2 \Pi(e^2; \varphi | e^2)}{a}, \quad (1)$$

where  $\Pi$  denotes the Legendre incomplete elliptic integral of the third kind defined by

$$\Pi(n; \varphi | m) = \int_0^\varphi \frac{dt}{(1 - n \sin^2 t) \sqrt{1 - m \sin^2 t}} \quad |\varphi| \leq \frac{\pi}{2}, \quad (2)$$

see APPENDIX A. Here  $\varphi$  is the geographic latitude of  $P$ <sup>1</sup>, and for the sake of simplicity, here and in what follows, we write  $\Pi(\cdot) \equiv \Pi(e^2; \cdot | e^2)$ , see [41]. The special function  $\Pi$  is

<sup>1</sup>According to the remark upon rhumb line course  $\alpha \neq 90^\circ$  we have [45, p. 134, Eq. (6)] that  $L_{lox} = L_m \cdot \sec \alpha$ . Therefore

$$L_{lox} = \frac{L_m}{\cos \alpha} = \frac{b^2 \Pi(\varphi)}{a \cdot \cos \alpha}.$$

For  $\alpha = 90^\circ$  we have equator, or parallel sailing, while for  $\alpha = 0^\circ$  it is  $L_{lox} \equiv L_m$ .

continuous and odd on the range  $|\varphi| \leq \pi/2$ , and being

$$\frac{d}{d\varphi} \Pi(n; \varphi|m) = \frac{1}{(1 - n \sin^2 \varphi) \sqrt{1 - m \sin^2 \varphi}} > 0 \quad n, m \in (0, 1),$$

it is monotone increasing function in  $\varphi$ . The monotonicity property implies invertibility, that is,  $w = \Pi(n; z|m)$  possesses an unique inverse  $z = \Pi^{-1}(n; w|m)$ . Now, by virtue of (1) we clearly conclude that the meridian distance between positions  $Q, P$  corresponds to the latitude

$$\varphi = \Pi^{-1}\left(\frac{a L_m}{b^2}\right). \quad (3)$$

Citations regarding inverse elliptic integral of the third kind are very rare; Allender–Hornreich–Johnson [3, p. 2655] refer to Saupe [43, p. 817, Eq. (7)] concerning the exact solution for the approximated Euler–Lagrange equation which describes the free energy of the uniformly distorted Fréedericksz state, remarking that the exact solution of approximated EL–equation “... it is expressed ... as an inverse elliptic function of the third kind. This is inconvenient for numerical calculations...”. They considered binomial type approximations for  $\Pi^{-1}(w) \approx C \cdot (1 - w^\rho)$ ,  $\rho$  real,  $C$  an absolute constant (see [3, p. 2657]). However, Saupe followed the usual computational way expressed in section 4.

Bearing in mind the fact that there is no explicit formula for  $\Pi$  and  $\Pi^{-1}$  expressed *via* certain elementary or higher transcendental functions, we are forced to compute it by numerical methods with prescribed accuracy. So, the meridian arc length  $L_m = L_m(\varphi)$  we compute by finding the associated  $\Pi$  function value in (1). Similarly, solving the inverse problem  $\Pi^{-1}$  in (3) we can calculate it only by certain numerical computation procedures that have the computation error under the prescribed accuracy level. Let us remark that e.g. the computational softwares contain built-in subroutines such as `EllipticPi[n, z, m]` in *Mathematica*. In the next chapters we will survey these questions with a list of related links.

### 3. COMPUTING $\Pi(\varphi)$ BY NUMERICAL QUADRATURES

To compute the meridian arc length  $L_m$ , reduce the problem to one of finding values of the elliptic integral of the third kind

$$\Pi(\varphi) = \int_0^\varphi \frac{dt}{(1 - e^2 \sin^2 t)^{3/2}}. \quad (4)$$

Based on a polynomial interpolation of the integrand using uniform grid, we calculate  $\Pi(\varphi)$  by certain of the familiar numerical quadratures such as Newton–Cotes formulae, represented by composite rectangle and trapezoidal rules (constant and linear approximation), Simpson’s formula (quadratic polynomial approximation); Gaussian quadrature formula and its numerous variants e.g. Gauss–Legendre, Gauss–Kronrod, Gauss–Lobatto rules etc. For instance,

the composite trapezoidal formula for  $\Pi(\varphi)$  is

$$\Pi(\varphi) = \frac{\varphi}{2n} \left\{ 1 + (1 - e^2 \sin^2 \varphi)^{-3/2} + 2 \sum_{j=1}^{n-1} \left[ \left( 1 - e^2 \sin^2 \left( \frac{\varphi j}{n} \right) \right)^{-3/2} \right] \right\} + R_n^T(\varphi), \quad (5)$$

where the error term is

$$R_n^T(\varphi) = \frac{3e^2 \varphi^3 [4(e^2 - 2) \cos(2\vartheta\varphi) + e^2(2 \cos(4\vartheta\varphi) - 7)]}{32n^2(1 - e^2 \sin^2(\vartheta\varphi))^{7/2}}, \quad \vartheta \in (0, 1).$$

Knowing the computation accuracy  $\varepsilon > 0$ , we can estimate the grids size  $n$  from  $R_n(\varphi) < \varepsilon$ , for any fixed  $\varphi$ . We mention that the composite Simpson's formula in our case reduces to

$$\begin{aligned} \Pi(\varphi) = \frac{\varphi}{6n} \left\{ 1 + (1 - e^2 \sin^2 \varphi)^{-3/2} + 4 \sum_{j=1}^{n-1} \left[ 1 - e^2 \sin^2 \left( \frac{\varphi j}{n} \right) \right]^{-3/2} \right. \\ \left. + 2 \sum_{j=1}^n \left[ 1 - e^2 \sin^2 \left( \frac{\varphi(2j-1)}{2n} \right) \right]^{-3/2} \right\} + R_n^S(\varphi), \end{aligned} \quad (6)$$

and the error term becomes

$$\begin{aligned} R_n^S(\varphi) &= \frac{\varphi^5}{2880 n^4} \left( (1 - e^2 \sin^2 t)^{-3/2} \right)' \Big|_{t=\xi} \\ &= \frac{3e^2 \varphi^5}{2880 n^4 (1 - e^2 \sin^2 \xi)^{11/2}} \left[ 11 e^6 \sin^8 \xi + 7.5 e^6 \sin^4(2\xi) - 18 e^4 \sin^6 \xi \right. \\ &\quad \left. + 2 \cos^2 \xi \cdot (52 e^6 \sin^6 \xi - e^4 \sin^4 \xi - 49 e^2 \sin^2 \xi - 2) \right. \\ &\quad \left. + 3e^2 \sin^4 \xi + 15 e^2 \cos^4 \xi \cdot (12 e^2 \sin^2 \xi + 1) + 4 \sin^2 \xi \right], \quad \xi \in (0, \varphi). \end{aligned}$$

Also by  $|R_n^S(\varphi)| < \varepsilon$  we evaluate  $n$  and then proceed to (6) with some fixed  $\varphi$ . We note that these two numerical quadratures are built-in [29].

Transforming the integration interval  $[0, \varphi]$ ,  $\varphi \leq \pi/2$  onto  $[-1, 1]$  putting  $\varphi(t+1)/2 \mapsto t$  in the integrand of (4), the Gauss-Legendre quadrature rule gives the approximation

$$\begin{aligned} \Pi(\varphi) &= \frac{\varphi}{2} \int_{-1}^1 \left[ 1 - e^2 \sin^2 \left( \frac{\varphi}{2}(t+1) \right) \right]^{-3/2} dt \\ &= \frac{\varphi}{2} \sum_{j=1}^n w_j \left[ 1 - e^2 \sin^2 \left( \frac{\varphi}{2}(t_j+1) \right) \right]^{-3/2} + R_n^{GL}(\varphi), \end{aligned}$$

where the weight-coefficients

$$w_j = \frac{2}{(1 - t_j^2)[P_n'(t_j)]^2}, \quad j = \overline{1, n}$$

are based on the Legendre polynomial  $P_n(x)$ , see APPENDIX C. The related quadrature error formula turns out to be

$$R_n^{GL}(\varphi) = \frac{(n!)^4 \varphi^{2n+1}}{(2n+1)[(2n)!]^3} \left( (1 - e^2 \sin^2 t)^{-3/2} \right)^{(2n)} \Big|_{t=\xi}, \quad \xi \in (0, \varphi).$$

For other kinds of Gaussian quadratures, e.g Gauss–Kronrod quadrature, we refer to the original Kronrod’s monograph [36]; also see the book [31] by Kahaner–Moler–Nash.

The Gauss–Lobatto quadrature is a kind of Gauss–Legendre quadrature procedure, since it is based on the Legendre polynomial  $P_n(x)$ . For more information please consult the celebrated work by Abramowitz–Stegun [1, pp. 888–900]. The related weights have been given up to  $n = 11$  in [15, pp. 63–64].

Gaussian quadrature is used in the QUADPACK library, the GNU Scientific Library, the NAG Numerical Libraries and statistical software *R*, see [28].

Also, we draw the mathematically better prepared reader’s attention to the excellent monograph by Gil–Segura–Temme [24, §5.3: Gauss quadrature].

#### 4. BINOMIAL SERIES EXPANSION OF THE INTEGRAND

The most common computational procedure concerns the binomial series expansion of the integrand in (1) (see e.g. Saupe’s paper [43]):

$$\begin{aligned} (1 - e^2 \sin^2 \varphi)^{-3/2} &= \sum_{n \geq 0} \binom{-3/2}{n} (-1)^n e^{2n} \sin^{2n} \varphi \\ &= 1 + \frac{3}{2} e^2 \sin^2 \varphi + \frac{15}{8} e^4 \sin^4 \varphi + \frac{35}{16} e^6 \sin^6 \varphi + \frac{315}{128} e^8 \sin^8 \varphi + \dots, \end{aligned} \quad (7)$$

the termwise integration applied after legitimate exchange the order of summation and integration gives the meridian distance  $L_m$  from the equator to a point  $P$  of latitude  $\varphi$  (the so-called Delambre expansion)

$$\begin{aligned} L_m = a(1 - e^2) \left\{ A\varphi - \frac{B}{2} \sin(2\varphi) + \frac{C}{4} \sin(4\varphi) \right. \\ \left. - \frac{D}{6} \sin(6\varphi) + \frac{E}{8} \sin(8\varphi) - \frac{F}{10} \sin(10\varphi) + \dots \right\}, \end{aligned} \quad (8)$$

where

$$\begin{aligned} A &= 1 + \frac{3}{4} e^2 + \frac{45}{64} e^4 + \frac{175}{256} e^6 + \frac{11\,025}{16\,384} e^8 + \frac{43\,659}{65\,536} e^{10} + \dots \\ B &= \frac{3}{4} e^2 + \frac{15}{16} e^4 + \frac{525}{512} e^6 + \frac{2\,205}{2\,048} e^8 + \frac{72\,765}{65\,536} e^{10} + \dots \\ C &= \frac{15}{64} e^4 + \frac{105}{256} e^6 + \frac{2\,205}{4\,096} e^8 + \frac{10\,395}{16\,384} e^{10} + \dots \\ D &= \frac{35}{512} e^6 + \frac{315}{2\,048} e^8 + \frac{31\,185}{131\,072} e^{10} + \dots \\ E &= \frac{315}{16\,384} e^8 + \frac{3\,465}{65\,536} e^{10} + \dots \\ F &= \frac{693}{131\,072} e^{10} + \dots \end{aligned}$$



Higher order partial sums in the expansion (7) gives additional concretized terms in (8), see e.g. [34, p. 1, Eq. (1)]. Deakin [17] reported that for the Geodetic Reference System 1980 (GRS80) ellipsoid ( $a = 6\,378.137$  [km];  $b = 6\,356.752\,314\,140$  [km])<sup>2</sup> the coefficients

$$\begin{aligned} A &= 1.005\,052\,501\,813\,087, & B &= 0.005\,063\,108\,622\,224 \\ C &= 0.000\,010\,627\,590\,263, & D &= 0.000\,000\,020\,820\,379 \\ E &= 0.000\,000\,000\,039\,324, & F &= 0.000\,000\,000\,000\,071. \end{aligned}$$

Therefore the corresponding meridian arc length approximation formula, with terms kept up to degree 10, reads

$$\begin{aligned} L_m^{80} &= 6\,367.449\,139\,507\,109\,\varphi - 16.038\,508\,725\,491\,\sin(2\varphi) + 0.016\,832\,613\,310\,\sin(4\varphi) \\ &\quad - 0.000\,021\,984\,375\,\sin(6\varphi) + 3.1\,142 \cdot 10^{-8}\,\sin(8\varphi) - 4.49 \cdot 10^{-11}\,\sin(10\varphi). \end{aligned} \quad (9)$$

Multiplying coefficients by  $1 - e^2$ , Lauf [37, p. 36] transformed formula (8) into

$$L_m = a \{ A_0\varphi - A_2\sin(2\varphi) + A_4\sin(4\varphi) - A_6\sin(6\varphi) + A_8\sin(8\varphi) + \dots \}, \quad (10)$$

where

$$\begin{aligned} A_0 &= 1 - \frac{1}{4}e^2 - \frac{3}{64}e^4 - \frac{5}{256}e^6 - \frac{175}{16\,384}e^8 + \dots \approx 0.998\,324\,298\,423\,043 \\ A_2 &= \frac{3}{8} \left( e^2 + \frac{1}{4}e^4 + \frac{15}{128}e^6 + \frac{35}{512}e^8 + \dots \right) \approx 0.002\,514\,607\,124\,555 \\ A_4 &= \frac{15}{256} \left( e^4 + \frac{3}{4}e^6 + \frac{35}{64}e^8 + \dots \right) \approx 0.000\,002\,639\,111\,298 \\ A_6 &= \frac{35}{3072} \left( e^6 + \frac{5}{4}e^8 + \dots \right) \approx 0.000\,000\,003\,446\,837 \\ A_8 &= \frac{315}{131\,072} \left( e^8 + \dots \right) \approx 0.000\,000\,000\,004\,883 \quad \text{etc.} \end{aligned}$$

Powers of  $e$  higher than  $e^6$  are ignored in (10). Thus, one obtains the official formula for meridian distance used by Geocentric Datum of Australia Technical Manual (ICSM 2002) [30]

$$\begin{aligned} \tilde{L}_m &= 6\,367.449\,145\,771\,052\,\varphi - 16.038\,508\,741\,588\,\sin(2\varphi) \\ &\quad + 0.016\,832\,613\,417\,\sin(4\varphi) - 0.000\,021\,984\,399\,\sin(6\varphi), \end{aligned} \quad (11)$$

which modestly differs from the  $L_m^{80}$  expression; also see [37, p. 36, Eq. (3.55)]<sup>3</sup>.

In 1837 the celebrated scholar Bessel [7] presented a meridian arc length formula, expressed in terms of the third flattening (or oblateness) of the globe ellipsoid  $n = (a - b)/(a + b)$  (not equal to the Legendre modulus characteristic in  $\Pi(n; \varphi|m)$ ). He rewrote (8) as

$$L_m^B = a(1 - n)^2(1 + n) \left\{ \left( 1 + \frac{9}{4}n^2 + \frac{225}{64}n^4 \right) \varphi - \left( \frac{3}{2}n + \frac{45}{16}n^3 + \frac{525}{128}n^5 \right) \sin(2\varphi) \right\}$$

<sup>2</sup>The currently used official WGS84 ellipsoid has equal  $a$ , but  $b = 6\,356.752\,314\,2$  [km]; this modest difference does not influence the navigations calculations.

<sup>3</sup>Deakin pointed out that at  $\varphi = 50^\circ$ , meridian distances calculated with (9) and by the formula  $\tilde{L}_m$  (11) differ for  $4.11 \cdot 10^{-4}$  [m], that is, "...GDA Technical Manual will give millimetre accuracy for latitudes covering Australia" [17].

$$+ \left( \frac{15}{16}n^2 + \frac{105}{64}n^4 \right) \sin(4\varphi) - \left( \frac{35}{48}n^3 + \frac{945}{768}n^5 \right) \sin(6\varphi) \Big\}, \quad (12)$$

The main advantage of (12) over the partial sum of order 10 of  $L_m$  in (8) is its good convergence, as  $n \approx e^2/4$ . Bessel's formula employed a reduced number of addends with approximately the same precision, see [34].

The German geodesist Helmert [25, pp. 44–48] gave an approximation formula for  $L_m \approx L_m^H$  expressed *via* the same ellipsoid parameter  $n$ . Consider the series expansion <sup>4</sup>

$$\begin{aligned} L_m = a(1-n)(1-n^2) & \left\{ \left( 1 + \frac{9}{4}n^2 + \frac{225}{64}n^4 + \dots \right) \varphi - \left( \frac{3}{2}n + \frac{45}{16}n^3 + \dots \right) \sin(2\varphi) \right. \\ & + \frac{1}{2} \left( \frac{15}{8}n^2 + \frac{105}{32}n^4 + \dots \right) \sin(4\varphi) - \frac{1}{3} \left( \frac{35}{16}n^3 + \dots \right) \sin(6\varphi) \\ & \left. + \frac{1}{4} \left( \frac{315}{128}n^4 + \dots \right) \sin(8\varphi) + \dots \right\}, \end{aligned}$$

Helmert multiplied coefficients by  $(1-n^2)^2$  and rejected all terms beginning with  $\sin(10\varphi)$ . He made use of truncated coefficients excluding all terms involving powers of  $n$  greater than  $n^4$  [18, p. 70, Eq. (226)], [34, p. 2, Eq. (6)]. Thus,

$$\begin{aligned} L_m^H = \frac{a}{1+n} & \left\{ \left( 1 + \frac{1}{4}n^2 + \frac{1}{64}n^4 \right) \varphi - \left( \frac{3}{2}n - \frac{3}{16}n^3 \right) \sin(2\varphi) \right. \\ & \left. + \left( \frac{15}{16}n^2 - \frac{15}{64}n^4 \right) \sin(4\varphi) - \frac{35}{48}n^3 \sin(6\varphi) + \frac{315}{512}n^4 \sin(8\varphi) \right\}. \quad (13) \end{aligned}$$

This alternative Helmert's formula is essentially the same as [5, p. 50, Eq. (5.5)].

A way to compute the latitude  $\varphi$  given a meridian arc length  $L_m$  was solved by Lauf [37, p. 38, Eq. (3.72)] by series inversion technique:

$$\begin{aligned} \varphi = \sigma + \left( \frac{3}{2}n - \frac{27}{32}n^3 + \dots \right) \sin(2\sigma) & + \left( \frac{21}{16}n^2 - \frac{55}{32}n^4 + \dots \right) \sin(4\sigma) \\ & + \left( \frac{151}{96}n^3 + \dots \right) \sin(6\sigma) + \left( \frac{1097}{512}n^4 - \dots \right) \sin(8\sigma) + \dots, \end{aligned}$$

where

$$\sigma = \frac{L_m}{G}, \quad G = a(1-n)(1-n^2) \left( 1 + \frac{9}{4}n^2 + \frac{225}{64}n^4 + \dots \right).$$

Here  $G$  stands for the mean length of a meridian arc of one radian, see also [18, p. 71, Eq. (229)].

Applying numerical root-finding routines like Newton–Raphson, secant, regula falsi, iteration etc. methods to Helmert's formula (13), we can perform numerical latitude computation with given accuracy, consult Deakin–Hunter's Newton–Raphson iteration MATLAB routines [18, pp. 107–119, §3.2].

Belyakov–Kravtsova–Rappaport [6, p. 5] used two standard power series in  $n$  and  $m$  to evaluate  $\Pi(n; \varphi|m)$ . Following their traces, and bearing in mind that we take  $n = m = e^2$ ,

<sup>4</sup>This series expansion in terms of  $n$  possesses a faster rate of convergence than the meridian distance formula (8) involving powers of  $e^2$ .

their power series coincide with

$$\Pi(\varphi) = \sum_{j=0}^{\infty} \frac{(2j)!}{(j!)^2} A(j) \left(\frac{e}{2}\right)^{2j} \quad (14)$$

$$= \sum_{j=0}^{\infty} \frac{(2j)!}{(j!)^2} B(j) \left(-\frac{b^2}{4a^2}\right)^j. \quad (15)$$

where

$$A(j) = \int_0^\varphi \frac{\sin^{2j} t}{1 - e^2 \sin^2 t} dt, \quad B(j) = \int_0^\varphi \frac{\sec t \tan^{2j} t}{1 - e^2 \sin^2 t} dt.$$

Because series (14) is not useful for numerical computation for  $e|\sin \varphi|$  near to 1 and series (15) slowly converges for  $ba^{-1}|\tan \varphi|$  close to 1<sup>5</sup>, Franke [20] reformulated the method by Ai–Harrison [2] to evaluate  $\Pi(\varphi)$  for a range of  $\varphi$  critical for the direct use of series (14), (15); he introduced the so-called "double-angle" approach remarking that "... *one application is sufficient for computational purposes*", see [20, p. 495].

We point out that by some longer routine calculation one arrives at

$$A(j) = \frac{\sin^{2j+1} \varphi}{2j+1} F_1\left(j + \frac{1}{2}; j+1, 1; j + \frac{3}{2}; \sin^2 \varphi, e^2 \sin^2 \varphi\right) \quad (16)$$

$$B(j) = \frac{\sin^{2j+1} \varphi}{2j+1} F_1\left(j + \frac{1}{2}; \frac{1}{2}, 1; j + \frac{3}{2}; \sin^2 \varphi, e^2 \sin^2 \varphi\right), \quad (17)$$

where both Appell's hypergeometric  $F_1$ -functions of two variables converge, being  $\Pi(\varphi)$  incomplete elliptic integral, that is,  $|\varphi| < \pi/2$ , consult APPENDIX B. Let us mention that  $F_1$  is built-in in *Mathematica*, having code `AppellF1[a, b_1, b_2, c, x, y]`, which evaluate  $F_1$ -values with the desired numerical precision inside the domain  $|x| < 1, |y| < 1$ . Now, approximating  $\Pi(\varphi)$  by a suitably long partial sum of series (14), (15) in conjunction with (16), (17), we conclude a new appropriate numerical evaluation tool.

Finally, the convergence rate problem obviously occurs caused by slowly convergent binomial series (7) and the subsequent trigonometric series concluded by termwise integration. So, these methods seem to be inefficient for general input argument values [12, 21]. Moreover, preliminary trials show that the approach using the theta functions [1], is also inferior to the computation procedures applying Gauss or Bartky transformations [21, p. 1963].

## 5. POWER SERIES EXPANSIONS

The Maclaurin series expansion of the integrand (7) leads to

$$\Pi(\varphi) = \varphi + \frac{3e^2}{2}\varphi^3 + \left(\frac{3e^4}{8} - \frac{e^2}{10}\right)\varphi^5 + \left(\frac{35e^6}{112} - \frac{5e^4}{28} + \frac{e^2}{105}\right)\varphi^7 + R_8^M(\varphi), \quad (18)$$

---

<sup>5</sup>Actually, computational problems occur already for  $ba^{-1}|\tan \varphi| \geq 0.7$ , [20, p. 495].

where the error term in the Lagrange form reads

$$R_8^M(\varphi) = \frac{\Pi^{(8)}(\vartheta\varphi)}{40\,320}\varphi^8, \quad \vartheta \in (0, 1).$$

The related Maclaurin polynomial gives the low order, therefore expectedly not too precise, approximation formula

$$L_m^M = \frac{b^2}{a} \left\{ \varphi + \frac{3e^2}{2}\varphi^3 + \left( \frac{3e^4}{8} - \frac{e^2}{10} \right) \varphi^5 + \left( \frac{35e^6}{112} - \frac{5e^4}{28} + \frac{e^2}{105} \right) \varphi^7 \right\}, \quad (19)$$

which turns out to be the truncated partial sum of the power series expansion presented in APPENDIX B - up to the constant  $b^2/a$ . Obviously, close-to-nil  $\varphi$  guarantees higher precision employing (19).

Completely different kinds of series expansion results are established by Karp–Savenkova–Sitnik [32, 33]. They considered  $\Pi(\varphi)$  on the range

$$\varphi \in \mathcal{D} = \left[ -\max \left\{ \frac{\pi}{2}, \arcsin \frac{a}{\sqrt{a^2 + b^2}} \right\}, \min \left\{ \frac{\pi}{2}, \arcsin \frac{a}{\sqrt{a^2 + b^2}} \right\} \right],$$

see [32, p. 334, Theorem 1]. Related worked examples can be found in [33].

## 6. BULIRSCH, AND FUKUSHIMA–ISHIZAKI METHODS

Bulirsch introduced a new way to compute all three elliptic integrals  $F, E, \Pi$  in both complete and incomplete cases. (However, we concentrate here only on his results regarding elliptic integral of the third kind). His approach is based on the Bartky's transformation (actually a by-product of the familiar Landen, or Gauss–Landen transformation) [10]. Bulirsch gave the routine:

$$el3(x, k_c, p) = \int_0^{\arctan x} \frac{d\gamma}{(\cos^2 \gamma + p \sin^2 \gamma) \sqrt{\cos^2 \gamma + k_c^2 \sin^2 \gamma}}, \quad |k_c| \leq 1, \quad (20)$$

where the main branch of the arctan is used, that is,  $|\arctan x| \leq \pi/2$ , and according to the notations introduced in (4),  $x, k_c, p$  correspond to  $\tan \varphi, \sqrt{1 - e^2}, 1 - e^2$  respectively. Consequently (compare APPENDIX A):

$$\Pi(\varphi) = el3(\tan \varphi, \sqrt{1 - e^2}, 1 - e^2).$$

The ALGOL procedure for  $el3$  is available from [11].

Having cancellation problems with the complementary characteristic  $p = 1 - n$  in  $el3$ , when the parameter  $|n|$  of  $\Pi(n; \varphi|m)$  is small, Bulirsch unified  $el3$  by [11, p. 279, Eq. (4.1.14)]

$$el(x, k_c, p, a, b) = \int_0^{\arctan x} \frac{(a \cos^2 t + b \sin^2 t) d\gamma}{(\cos^2 \gamma + p \sin^2 \gamma) \sqrt{\cos^2 \gamma + k_c^2 \sin^2 \gamma}}, \quad |k_c| \leq 1.$$



He did not give a related computation routine. Fukushima–Ishizaki extended  $el(\cdot)$  to the ‘incomplete’ routine function [23, p. 240, Eq. (21)]

$$G(\varphi, n_c, m_c, a, b) = \int_0^\varphi \frac{(a \cos^2 \gamma + b \sin^2 \gamma) d\gamma}{(\cos^2 \gamma + n_c \sin^2 \gamma) \sqrt{\cos^2 \gamma + m_c \sin^2 \gamma}}, \quad (21)$$

where parameters  $n_c, m_c$  were introduced to avoid a loss of precision. Hence, they solved the cancellation problem with respect to  $n$  positively [23].

Obviouly (consult APPENDIX A)

$$\Pi(\varphi) = G(\varphi, 1 - e^2, 1 - e^2, 1, 1).$$

The complete description of the Fukushima–Ishizaki routine and the calculation algorithm is presented with companion numerical examples in [23].

## 7. DUPLICATION METHOD BY CARLSON

We have mentioned that Franke initiates a kind of duplication of angles in computing  $\Pi(\varphi)$  with a desired accuracy, [20]. In a set of articles, see [13] and his references [3, 4, 5, 6] therein, Carlson developed a new approximation method by introducing a new set of so-called  $R$ -integrals in the standardized form. Concentrating on  $\Pi(\varphi)$ , the adequate standard Carlson integrals of the first and the third kind are [13, p. 2, Eqs. (1.1),(1.3)]

$$\begin{aligned} R_F(x, y, z) &= \frac{1}{2} \int_0^\infty [(t+x)(t+y)(t+z)]^{-1/2} dt \\ R_J(x, y, z, \rho) &= \frac{3}{2} \int_0^\infty [(t+x)(t+y)(t+z)]^{-1/2} (t+\rho)^{-1} dt, \quad \rho \neq 0. \end{aligned}$$

These functions are symmetric in  $x, y, z$  and normalized so, that  $R_F(x, x, x) = x^{-1/2}$ , while  $R_J(x, x, x, x) = x^{-3/2}$  and  $R_J(0, y, z, \rho)$  is said to be complete. Two cases are signified as

$$R_C(x, y) = R_F(x, y, y), \quad R_D(x, y, z) = R_J(x, y, z, z). \quad (22)$$

The variables  $x, y, z$  are nonnegative and at most one of them is zero<sup>6</sup>. The link to  $\Pi(\varphi)$  is [13, p. 8, Eq. (4.3)]

$$\Pi(\varphi) = \sin \varphi \cdot R_F(\cos^2 \varphi, 1 - e^2 \sin^2 \varphi, 1) + \frac{e^2}{3} \sin^3 \varphi \cdot R_D(\cos^2 \varphi, 1 - e^2 \sin^2 \varphi, 1). \quad (23)$$

The connection with Bulirsch  $el3$  procedure becomes

$$\begin{aligned} \Pi(\varphi) &= el3(\tan \varphi, \sqrt{1 - e^2}, 1 - e^2) = \tan \varphi \cdot R_F\left(1, \frac{1 - e^2 \sin^2 \varphi}{\cos^2 \varphi}, \frac{1}{\cos^2 \varphi}\right) \\ &\quad + \frac{1 - e^2}{3} \tan^3 \varphi \cdot R_D\left(1, \frac{1 - e^2 \sin^2 \varphi}{\cos^2 \varphi}, \frac{1}{\cos^2 \varphi}\right). \end{aligned}$$

<sup>6</sup>We have to point out that Carlson’s set of  $R$ -integrals cover a wide family of logarithmic, inverse circular, inverse hyperbolic functions, complete and incomplete elliptic integrals as special cases [13, §4].

Bearing in mind (23), we have to expose Carlson's computation procedure for the duplication formulae [14, Eqs. 19.26.18–19, 22–23]

$$R_F(x, y, z) = 2R_F(x + \lambda, y + \lambda, z + \lambda) = R_F\left(\frac{x + \lambda}{4}, \frac{y + \lambda}{4}, \frac{z + \lambda}{4}\right) \quad (24)$$

$$R_D(x, y, z) = 2R_D(x + \lambda, y + \lambda, z + \lambda) + \frac{3}{\sqrt{z}(z + \lambda)}, \quad (25)$$

where

$$\lambda = \sqrt{xy} + \sqrt{xz} + \sqrt{yz}.$$

After the differences between the variables have been made enough small by successive duplications by (24) and (25), the integrals  $R_F, R_D$  are expanded into a triple Maclaurin series approximated by their partial sums of order five. The resulting algorithms consist only of rational operations and square roots. The convergence is fast enough to be superior to methods possessing second order convergence, unless extremely high precision is required, [13, p. 2]. The related algorithms for  $R_F, R_C, R_J, R_D$  are given respectively in [13, pp. 2–5, **Algorithm 1-4.**], but they are too massive to be presented here in detail.

## 8. $J$ -FUNCTION METHOD BY FUKUSHIMA.

Guided by certain practical reasons such as avoiding the loss of significant digits for small  $|n|$ , Fukushima [21] introduced a linear combination of the Legendre's incomplete elliptic integrals of the first (see APPENDIX A) and third kind instead of  $\Pi(n; \varphi|m)$  itself:

$$J(n; \varphi|m) = \frac{1}{n} (\Pi(n; \varphi|m) - F(\varphi|m)) \quad \varphi \in \left(0, \frac{\pi}{2}\right), m, n \in (0, 1),$$

calling it *associated incomplete elliptic integral of the third kind*. Obviously, knowing  $J(n; \varphi|m)$  and  $F(\varphi|m)$  we have

$$\Pi(n; \varphi|m) = F(\varphi|m) + nJ(n; \varphi|m).$$

Fukushima outlined [21, p. 1963, §1.3] that the standard computation methods employed for  $J(n; \varphi|m)$  are Bulirsch's, and Carlson's (applied to  $R_J$ ). However, from the practical point of view, both methods suffer from either cancellation errors or from large amounts of computation, see the discussions around [21, p. 1964, Eqs. (19), (21)]; the comparison to Bulirsch's and Carlson's methods are given in [21, §4].

Fukushima's  $J$ -method is based on selecting one function from the four possible expressions:

$$J(n; \varphi|m) = \begin{cases} J(n; \varphi|m) & \text{(i)} \\ J(n|m) - J\left(n; \arcsin \frac{\cos \varphi}{\sqrt{1 - n \sin^2 \varphi}} \middle| m\right) - R_C(t_s^{-2}, h + t_s^{-2}) & \text{(ii)} \\ J(n|m) - J\left(n; \arccos \sqrt{\frac{1 - m}{1 - m \sin^2 \varphi}} \middle| m\right) - R_C(t_c^{-2}, h + t_c^{-2}) & \text{else} \end{cases}$$

where  $J(n|m) = J(n; \pi/2|m)$  is the associate complete elliptic integral of the third kind and

$$\begin{cases} \text{(i)} & \varphi < \varphi_s \quad \text{or} \quad \varphi > \arcsin \frac{1}{\sqrt{\sqrt{1+m}+1}} \\ \text{(ii)} & \frac{\cos \varphi}{\sqrt{1-n \sin^2 \varphi}} < y_s \end{cases},$$

while

$$h = n(1-n)(n-m), \quad t_s = \frac{\sin(2\varphi)}{2\sqrt{1-m \sin^2 \varphi}}, \quad t_c = \frac{t_s}{1-n}.$$

Also,  $y_s, \varphi_s$  are constants, where  $y_s \in \{0.95, 0.90\}$  in the single and double precision computation modalities respectively, while  $\varphi_s = \arcsin \sqrt{y_s} \in \{1.345, 1.249\}$ .

In our environment writing  $J(\varphi) \equiv J(e^2; \varphi|e^2)$ ,  $J(e^2) \equiv J(\pi/2)$ ;  $F(\varphi) = F(\varphi|e^2)$ , we get the associate incomplete elliptic integral of the third kind

$$J(\varphi) = \frac{1}{n} (\Pi(\varphi) - F(\varphi)), \quad (26)$$

and the associated mathematical model

$$J(\varphi) = \begin{cases} J(\varphi) & \text{(i)} \\ J(e^2) - J\left(\arcsin \frac{\cos \varphi}{\sqrt{1-e^2 \sin^2 \varphi}}\right) - \frac{\sin(2\varphi)}{2\sqrt{1-e^2 \sin^2 \varphi}} & \text{(ii)} \\ J(e^2) - J\left(\arccos \frac{b}{a\sqrt{1-e^2 \sin^2 \varphi}}\right) - \frac{\sin(2\varphi)}{2(1-e^2)\sqrt{1-e^2 \sin^2 \varphi}} & \text{otherwise} \end{cases} \quad (27)$$

for

$$\begin{cases} \text{(i)} & \varphi < \varphi_s \quad \text{or} \quad \varphi > \arcsin \frac{1}{\sqrt{\sqrt{1+e^2}+1}} \\ \text{(ii)} & \frac{\cos \varphi}{\sqrt{1-e^2 \sin^2 \varphi}} < y_s \end{cases}.$$

Indeed,  $h = 0$  and  $R_C(x, x) = R_F(x, x, x) = x^{-1/2}$ , according to (22). Now, it remains to apply Fukushima's half and double argument transformations [21, pp. 1966–1970, §3.3–3.7] to the model (26) to earn the desired value of  $J(\varphi)$  for  $\varphi$  already given.

## 9. LUKE'S PADÉ APPROXIMATION METHOD

Using Padé <sup>7</sup> approximations for the square root, Luke [38, 39] offered routines for the approximative evaluation of elliptic integrals of all three kinds. His expression looks like (in our setting  $n = m = e^2$ ) [39, p. 193, Eqs. (26)]:

$$\Pi(\varphi) = \frac{H(\varphi, e^2)}{2n+1} \left\{ 1 + \sum_{j=1}^n \frac{2}{\cos^2 \frac{j\pi}{2n+1}} \right\}$$

<sup>7</sup>Henri Eugène Padé (1863–1953) a French mathematician who made important contributions to the theory of continued fractions and introduced what we call today Padé approximants, which are rational approximations to functions given by their power series.

$$\begin{aligned}
& -\frac{2}{2n+1} \sum_{j=1}^n H\left(\varphi, e^2 \sin^2 \frac{j\pi}{2n+1}\right) \tan^2 \frac{\pi j}{2n+1} + R_n^L(\varphi) \\
H(\tau, f) &= \frac{a}{b} \arctan\left(\frac{b}{a} \tan \tau\right) \\
R_n^L(\varphi) &= \frac{2e^{-(2n+1)\zeta} \tan \varphi}{(1-e^2 \sin^2 \varphi)(4n+3)} \left\{1 + \frac{\lambda_1}{4n+3} + \mathcal{O}(n^{-2})\right\} + \mathcal{O}(e^{-4n\zeta}) \\
\lambda_1 &= 1 - \frac{\cosh \zeta - 1}{\sinh \zeta \cdot \cos^2 \varphi} - \frac{2e^2 \sin^2 \varphi \cdot (\cosh \zeta - 1)}{(1-e^2 \sin^2 \varphi) \sinh \zeta}.
\end{aligned}$$

Here  $R_n^L(\varphi)$  is the error term which vanishes with growing  $n$  [39, p. 194, Eq. (28)]:

$$\lim_{n \rightarrow \infty} R_n^L(\varphi) = 0,$$

and  $e^\zeta$  is defined by [39, p. 191]

$$e^\zeta = \frac{2 - e^2 \sin^2 \varphi + 2\sqrt{1 - e^2 \sin^2 \varphi}}{e^2 \sin^2 \varphi}.$$

We are drawing the reader's attention to the important difference in notations of the base of natural logarithms  $e$ , and the eccentricity  $e$ .

A further variant of this method, useful for  $\varphi$  near to  $\pi/2$ , was proposed in [39, pp. 194–196, Eqs. (29)–(40)].

## 10. COMPARISON OF THE PRESENTED METHODS

Illustration of the presented methods will be the comparison of meridian distance calculation's efficiency for composite trapezoidal (5) and Simpson's (6) rules for few subdivisions  $n$ . These employ Geodetic Reference System 1980 (GRS80) ellipsoid formula  $L_m^{80}$  (9), Geocentric Datum of Australia Technical Manual (ICSM 2002) official formula  $\tilde{L}_m$  (11), Bessel's  $L_m^B$  (12), Helmert's  $L_m^H$  (13) formulae, and the power series approximation formula  $L_m^M$  (18), using referent values of WGS84 ellipsoid characteristics  $a = 6378.137$  [km],  $e = 0.0818192$  and the latitude of Senj <sup>8</sup>  $\varphi(S) = 45^\circ$  N. The corresponding value

$$\Pi(\pi/4) = \text{EllipticPi}[0.006694381, \pi/4, 0.006694381] = 0.786834838411$$

was evaluated by the **WolframAlpha** computational engine. By (1) we get <sup>9</sup>

$$L_m = a(1 - e^2)\Pi(\pi/4) = 4984.944374286 \quad [km] = 2691.654630 \quad [M].$$

<sup>8</sup>Senj is a small town situated on the Adriatic coast near Rijeka, Croatia.

<sup>9</sup>Here and in what follows, all computed values of meridian distances are expressed in [km] units; by  $L_m$  [km] =  $L_m/1.852$  [M] we clearly transform it into nautical miles.

First, by obvious rough estimates  $1 - e^2 \sin^2(\vartheta\varphi) \geq \cos^2(\vartheta\varphi) \geq \cos^2 \varphi$ , which hold true for all  $\varphi \in (0, \pi/2)$ ,  $\vartheta \in (0, 1)$ , we conclude that

$$\begin{aligned} |R_n^T(\pi/4)| &\leq \left. \frac{3e^2(13e^2 + 8)\varphi^3}{32n^2 \cos^7 \varphi} \right|_{\varphi=\frac{\pi}{4}} = \frac{0.003\,430}{n^2} \\ |R_n^S(\pi/4)| &\leq \left. \frac{e^2\varphi^5(122.5e^6 + 200e^4 + 116e^2 + 4)}{960n^4 \cos^{11} \varphi} \right|_{\varphi=\frac{\pi}{4}} = \frac{0.000\,828\,557}{n^4}. \end{aligned}$$

Denote  $L_m^T, L_m^S$  the right-hand-side sums in the trapezoidal (5) and Simpson's (6) rules, respectively. We get the following table

| $n$ | $L_m^T$      | $ R_n^T  <$     | $L_m^S$      | $ R_m^s  <$      |
|-----|--------------|-----------------|--------------|------------------|
| 2   | 4985.777 412 | $8.6 * 10^{-4}$ | 4984.907 385 | $5.2 * 10^{-5}$  |
| 3   | 4985.312 473 | $3.8 * 10^{-4}$ | -            | -                |
| 4   | 4985.151 015 | $2.1 * 10^{-4}$ | 4984.942 218 | $3.2 * 10^{-6}$  |
| 5   | 4985.076 504 | $1.3 * 10^{-4}$ | -            | -                |
| 6   | 4985.036 084 | $9.5 * 10^{-5}$ | 4984.943 954 | $6.4 * 10^{-7}$  |
| 10  | 4984.977 367 | $3.4 * 10^{-5}$ | 4984.944 321 | $8.3 * 10^{-8}$  |
| 20  | 4984.952 620 | $8.6 * 10^{-6}$ | 4984.944 372 | $5.2 * 10^{-9}$  |
| 50  | 4984.945 696 | $1.4 * 10^{-6}$ | 4984.944 372 | $1.3 * 10^{-10}$ |

Table 1. TRAPEZOIDAL AND SIMPSON'S RULES CALCULATIONS OF MERIDIAN DISTANCES

Next, we approximate  $L_m$  by  $L_m^{80}, \tilde{L}_m, L_m^B$  and  $L_m^H$  by quoted formulae (9), (11), (12) and (13) respectively. First, the third flattening parameter of the globe WGS84 ellipsoid is equal to

$$n = \frac{a - b}{a + b} = 0.001\,679\,220.$$

This value, together with the associated eccentricity  $e$  transforms Bessel's, Helmert's and the Maclaurin expansion formulae into

$$\begin{aligned} L_m^B &= 6\,367.449\,148\,277\,502\,\varphi - 16.038\,504\,978\,751\,\sin(2\varphi) \\ &\quad + 0.016\,832\,605\,426\,\sin(4\varphi) - 0.000\,021\,984\,392\,\sin(6\varphi) \\ L_m^H &= 6\,367.449\,148\,277\,505\,\varphi - 16.038\,504\,978\,753\,\sin(2\varphi) \\ &\quad + 0.016\,832\,605\,523\,\sin(4\varphi) - 0.000\,021\,984\,408\,\sin(6\varphi) \\ &\quad + 0.000\,000\,031\,148\,\sin(8\varphi) \\ L_m^M &= 6\,335.432\,364\,595\,861\,\varphi + 63.617\,697\,072\,503\,\varphi^3 \\ &\quad - 2.999\,026\,589\,075\,\varphi^5 + 0.353\,815\,715\,411\,\varphi^7. \end{aligned}$$

Latitude  $\varphi = 45^\circ$  of Senj gives

$$L_m^{80} = 4\,984.944\,373 \quad [km], \quad \tilde{L}_m = 4\,984.944\,378 \quad [km]$$

$$L_m^B = L_m^H = 4\,984.944\,384 \quad [km], \quad L_m^M = 5\,005.826\,977 \quad [km].$$

Now, it is not hard to see all estimated values of  $L_m$  differ in  $12 [mm]$ ; exceptions are the composite trapezoidal formula with approximately  $1.3 [m]$  deviation, and the very slowly convergent Maclaurin polynomial approximant  $L_m^M$  with near to  $21 [km]$  overlength. Therefore we conclude that all exposed and successfully examined formulae have the same navigational and geodesical significance and applicability.

## 11. CONCLUSION

In this article we presented, without using further computation, methods by Burlisch, Carlson, Fukushima–Ishizaki and Fukushima, since they are superior to the classical series expansion computation methods for the incomplete elliptic integral of the third kind  $\Pi(\varphi)$ .

The use of all presented methods is highly appreciated in numerous applications, because  $\Pi(n; \varphi|m)$  appears in various mathematical models. These include the approximated Euler–Lagrange equation [3, p. 2655], [43, p. 817, Eq. (7)], the model of the gravitational or electromagnetic field associated with scalar or vector potential of a simple distribution such as annular disks with finite thickness [21]; the model of a magnetic field caused by thick coil [19]; the torque-free rotation of triaxial rigid body [22, Appendix C] and the periodic solutions of the Schrödinger equation [16].

Our main purpose here was to present enough precise computational tools and procedures for navigational calculations in both nautical and geodesical topics. Regarding nautical themata, has to be mentioned the very recent article by Weintrit–Kopacz [44] in which the authors gave an exhaustive up-to-date presentation, together with the numerous articles therein e.g. [46, 47]. We point out that all these articles work with formulae and routines in terms of the geographic latitude  $\varphi$ , the exception is Petrović’s note [42], where the meridian arc length has been expressed *via* the incomplete elliptic integral of the second kind as  $L_m = a \cdot E(\theta|e^2)$ , see [42, p. 88, Eq. (21)], also see the paper by Kos–Filjar–Hess [35, p. 959].

## ACKNOWLEDGEMENTS

Both authors were partially supported by the *Ministry of Science, Education and Sports of the Republic of Croatia* under Research Projects No. 112-1121722-3066 and No. 112-1121722-3314, respectively.

## References

- [1] Abramowitz, M., Stegun, I.A. (Eds.) (1972). *Handbook of Mathematical Functions with Formulas, Graphs, and Mathematical Tables*. 9th printing. Dover, New York.
- [2] Ai, D.K., Harrison, Z.L. (1964). A computer method for calculating the complete and incomplete elliptic integrals of the third kind. Report AD-437-207. California Institute of Technology.

- [3] Allender, D.W. Hornreich, R.M., Johnson D.L. (1987). Theory of the stripe in bend-Fréedericksz-geometry nematic films. *Physical Review Letters* **59**, No. 23, 2654–2657.
- [4] Andrews, G.E., Askey, R., Roy, R. (1999). *Special Functions*. Encyclopedia of Mathematics and its Applications, 71. Cambridge University Press, Cambridge.
- [5] Baeschlin, C.F. (1948). *Lehrbuch Der Geodäsie*. Orell Füssli Verlag, Zürich.
- [6] Belyakov, V.M., Kravtsova, P.I., Rappoport, M.G. (1965). *Tables of Elliptical Integrals*. Part I. Mathematical Tables Series, Vol. 37. A Pergamon Press Book The Macmillan Co., New York.
- [7] Bessel, F.W. (1837). Bestimmung der Axen des elliptischen Rotationssphäroids, welches den vorhandenen Messungen der Meridianbögen der Erde am meistens entspricht. *Astronomische Nachrichten* **14**, 333–346.
- [8] Bulirsch, R. (1965). Numerical calculation of elliptic integrals and elliptic functions. *Numerische Mathematik* **7**, 78–90.
- [9] Bulirsch, R. (1965). Numerical calculation of elliptic integrals and elliptic functions II. *Numerische Mathematik* **7**, 353–354.
- [10] Bulirsch, R. (1969). An extension of Bartky–transformation to incomplete elliptic integrals of the third kind. *Numerische Mathematik* **13**, 266–284.
- [11] Bulirsch, R. (1969). Numerical calculation of elliptic integrals and elliptic functions III. *Numerische Mathematik* **13**, 305–315.
- [12] Byrd, P.F., Friedman, M.D. (1971). *Handbook on Elliptic Integrals for Engineers and Physicists*. 2nd ed. Springer–Verlag, Berlin.
- [13] Carlson, B.C. (1979). Computing elliptic integrals by duplication. *Numerische Mathematik* **33**, 1–16.
- [14] Carlson, B.C. (2010). Chapter 19. *Elliptic Integrals*. In Olver, F.W.J., Lozier, D.W., Boisvert, R.F., Clark, C.W. (Eds.) *Handbook of Mathematical Functions*. Cambridge University Press, Cambridge. Available at [<http://dlmf.nist.gov/19>]
- [15] Chandrasekhar, S. (1960). *Radiative Transfer*. Dover, New York.
- [16] Chow, K.W., Ng, T.W. (2011). Periodic solutions of a derivative nonlinear Schrödinger equation; elliptic integrals of the third kind. *Journal of Computational and Applied Mathematics* **235**, 3825–3830.
- [17] Deakin, R.E. (2006). Meridian distance. Unpublished manuscript, 30pp. Available online at [<http://user.gs.umat.edu.au/rod/files/publications>]
- [18] Deakin, R.E., Hunter, M.N. (2010). *Geometric Geodesy. Part A*. Second printing. RMIT University Melbourne, Australia.
- [19] Delinchant, B., Wurtz, F., Yonnet, J.-P., Coulomb, J.-L. (2011). Interaction between ring-shaped permanent magnets with symbolic gradients; application to magnetic bearing system optimization. *IEEE Transactions on Magnetics* **47**, 1418–1421.
- [20] Franke, C.H. (1965). Numerical evaluation of the elliptic integral of the third kind. *Mathematics of Computation* **19**, 494–496.
- [21] Fukushima, T. (2012). Precise and fast computation of a general incomplete elliptic integral of third kind by half and double argument transformations. *Journal of Computational and Applied Mathematics* **236**, 1961–1975.
- [22] Fukushima, T. (2008). Simple, regular and efficient numerical integration of rotational motion. *Astronomical Journal* **135**, 2298–2322.
- [23] Fukushima, T., Ishizaki, H. (1994). Numerical computation of incomplete elliptic integrals of a general form. *Celestial Mechanics and Dynamical Astronomy* **59**, 237–251.
- [24] Gil, A., Segura, J., Temme, N.M. (2007). *Numerical Methods for Special Functions*. Society for Industrial and Applied Mathematics (SIAM), Philadelphia, PA.
- [25] Helmert, F.R. (1880). *Die mathematischen und physikalischen Theorien der höheren Geodäsie. I. Teil. Die mathematischen Theorien*. Druck und Verlag B.G. Teubner, Leipzig.
- [26] <http://functions.wolfram.com/EllipticIntegrals/EllipticPi3/03/01/01/0006>
- [27] <http://functions.wolfram.com/EllipticIntegrals/EllipticPi3/06/01/07/0002>
- [28] <http://stat.ethz.ch/R-manual/R-patched/library/stats/html/integrate.html>
- [29] <http://www.zweigmedia.com/RealWorld/integral/integral.html>



- [30] ICSM. (2002). Geocentric Datum of Australia Technical Manual. Intergovernmental Committee on Surveying & Mapping (ICSM), Version 2.2, February 2002. [[www.anzlic.org.au/icsm/gdatum](http://www.anzlic.org.au/icsm/gdatum)]
- [31] Kahaner, D., Moler, C., Nash, S. (1989). *Numerical Methods and Software*. Prentice-Hall, Englewood Cliffs, NJ.
- [32] Karp, D., Savenkova, A., Sitnik, S.M. (2007). Series expansions for the third incomplete elliptic integral via partial fraction decompositions. *Journal of Computational and Applied Mathematics* **207**, No. 2, 331–337.
- [33] Karp, D., Savenkova, A., Sitnik, S.M. (2006). Series expansions for the third incomplete elliptic integral via partial fraction decompositions. [<http://arxiv.org/abs/math/0410009>], 11pp.
- [34] Kawase, K. (2011). A general formula for calculating meridian arc length and its application to coordinate conversion in the Gauss-Krüger projection. *Bulletin of the Geospatial Information Authority of Japan* **59**, December, 1–13.
- [35] Kos, S., Filjar, R., Hess, M. (2009). Differential equation of the loxodrome on a rotational surface. *Proceedings of the 2009 International Technical Meeting of the Institute of Navigation*. Anaheim, CA January 2009, 958–960.
- [36] Kronrod, A.S. (1965). *Nodes and Weights of Quadrature Formulas. Sixteen-place Tables*. Authorized translation from the Russian. Consultants Bureau, New York.
- [37] Lauf, G.B. (1983). *Geodesy and Map Projections*. 2nd ed. TAFE Publications Unit, Collingwood, Victoria, Australia.
- [38] Luke, Y.L. (1968). Approximations for elliptic integrals. *Mathematics of Computation* **22** 627–634.
- [39] Luke, Y.L. (1970). Further approximations for elliptic integrals. *Mathematics of Computation* **24** 191–198.
- [40] Mathai, A.M., Saxena, R.K. (1978). *The H-function with Applications in Statistics and other Disciplines*. Wiley Eastern Limited, New Delhi · Bangalore · Bombay.
- [41] Meyer, T.H., Rollins, C. (2011). The direct and indirect problem for loxodromes. *Navigation* **58**, No. 1, 1–6.
- [42] Petrović, M. (2007). Differential equation of a loxodrome on the spheroid. *Naše More* **54**, No. 3–4, 87–89.
- [43] Saupe, A. (1960). Die Biegeelastizität der nematischen Phase von Azoxyanisol. *Zeitschrift für Naturforschung* **15**, 815–822.
- [44] Weinrit, A., Kopacz, P. (2011). Geodesic based trajectories in navigation. *Coordinates* **VII**, No. 6. [<http://mycoordinates.org/geodesic-based-trajectories-in-navigation>]
- [45] Williams, J.E.D. (1950). Loxodromic distances on terrestrial spheroid. *The Journal of Navigation* **3**, No. 2, 133–140.
- [46] Williams, R., Phythian, J.E. (1989). Navigating along geodesic paths on the surface of a spheroid. *The Journal of Navigation* **42**, No. 1, 129–136.
- [47] Williams, R., Phythian, J.E. (1992). The shortest distance between two nearly antipodean points on the surface of a spheroid. *The Journal of Navigation* **45**, No. 1, 114–125.

APPENDIX A. To express  $L_m$  explicitly, we employ the Legendre’s incomplete elliptic integrals of the first, second and third kind defined respectively by

$$\begin{aligned}
 F(z|m) &= \int_0^z \frac{dt}{\sqrt{1-m\sin^2 t}} \\
 E(z|m) &= \int_0^z \sqrt{1-m\sin^2 t} dt \\
 \Pi(n; z|m) &= \int_0^z \frac{dt}{(1-n\sin^2 t)\sqrt{1-m\sin^2 t}} \quad |z| \leq \frac{\pi}{2};
 \end{aligned}$$

related functions

$$F\left(\frac{\pi}{2} \middle| m\right) = F(m), \quad E\left(\frac{\pi}{2} \middle| m\right) = E(m), \quad \Pi\left(n; \frac{\pi}{2} \middle| m\right) = \Pi(n|m)$$

signify the complete elliptic integrals of all three kinds. Because the function  $\Pi$  is odd and quasi-periodic, the following properties hold [26]

$$\begin{aligned} \Pi(n; z|m) &= -\Pi(n; -z|n) \\ \Pi(n; z + k\pi|m) &= \Pi(n; z|m) + k \Pi(n|m), \quad k \in \mathbb{Z}, |n| \leq 1 \\ \Pi(0; z|m) &= F(z|m) \\ \Pi(n; z|n) &= \frac{1}{1-n} \left\{ E(z|n) - \frac{n \sin(2z)}{2\sqrt{1-n \sin^2 z}} \right\}. \end{aligned}$$

The transcendental equation  $\Pi(n; z|n) = w$  has no explicit solution in  $z$ .

Rewriting (2) as

$$\Pi(n; \varphi|m) = \int_0^\varphi \frac{(\sin^2 t + \cos^2 t) dt}{(\cos^2 t + (1-n) \sin^2 t) \sqrt{\cos^2 t + (1-m) \sin^2 t}},$$

then introducing general parameters  $p = 1 - n, k_c^2 = 1 - m, x = \tan \varphi$ , Burilich in [8, 9, 10, 11], subsequently  $a, b, n_c = 1 - n, m_c = 1 - m$ , Fukushima-Ishizaki in [23] have proposed more general and redirected computation routines  $el3$  (20) and  $G$  (21) respectively, for the incomplete elliptic function of the third kind  $\Pi$ .

APPENDIX B. The Maclaurin series expansion of the elliptic integral of the third kind coincides with a triple series [27]

$$\begin{aligned} \Pi(n; \varphi|m) &= \frac{\sqrt{\pi} (m/2)^{3/2}}{n(m - 2(1 + \sqrt{1-m}))^{3/2} \sqrt{1-n}} \sqrt{1 + \frac{1}{\sqrt{1-m}}} \sum_{q=0}^{\infty} \frac{(-4)^q}{(2q+1)!} \sum_{k=0}^{2q} \frac{S_{2q}^{(k)}}{2^k} \\ &\times \sum_{j=0}^k \frac{(-n)^{-j} j! \binom{k}{k-j}}{\Gamma(j - k + \frac{1}{2})} \frac{m^{k-j} ((1 + \sqrt{1-n})^{j+1} - (1 + \sqrt{1-n})^{j+1})}{(1 - \sqrt{1-m})^{k-j}} \\ &\times F_1\left(\frac{1}{2}; \frac{1}{2}, -\frac{3}{2}; j - k + \frac{1}{2}; \frac{1}{2} - \frac{1}{2\sqrt{1-m}}, 2 \frac{1 + \sqrt{1-m}}{m}\right) \varphi^{2q+1}, \end{aligned}$$

where the Stirling numbers of the second kind

$$S_b^{(a)} = \frac{(-1)^a}{a!} \sum_{m=0}^a (-1)^m \binom{a}{m} m^b, \quad a, b - 1 \in \mathbb{N}$$

and the Appell function [40, p. 21, Eq. (2.1.1)]

$$F_1(a; b, b'; c; x, y) = \sum_{r,s=0}^{\infty} \frac{(a)_{r+s} (b)_r (b')_s}{(c)_{r+s} r! s!} x^r y^s, \quad |x| < 1, |y| < 1,$$

play significant roles. Here the familiar Pochhammer symbol (or shifted factorial)

$$(a)_n = a(a+1)\cdots(a+n-1) \quad a \in \mathbb{C}, n \in \mathbb{N}_0 = \{0, 1, 2, \dots\},$$

and  $0_0 = 1$  is used by convention. Specifying  $n = m = e^2$ , the previous formulae give (5).

APPENDIX C. The Legendre polynomial  $y = P_n(x)$  is a solution of the Legendre differential equation, reads as follows

$$((1-x^2)y')' + n(n+1)y = 0;$$

the solution may be expressed by the Rodrigues formula [4, p. 252]

$$P_n(x) = \frac{(-1)^n}{2^n n!} \frac{d^n}{d^n x} (1-x^2)^n.$$

The associated Gauss–Legendre low order ( $n = 1, 2, 3, 4$ ) quadrature weight–coefficients

$$w_j = \frac{2}{(1-t_j^2)[P'_n(t_j)]^2}, \quad j = \overline{1, n}, \quad n = 1, 2, 3, 4$$

are presented on the following table

| $n$ | nodes $t_j$  | weights $w_j$  |
|-----|--|--|
| 1   | 0  | 2  |
| 2   | $\pm \frac{1}{\sqrt{3}}$   | 1  |
| 3   | $\pm \sqrt{\frac{3}{5}}; 0$  | $\frac{5}{9}; \frac{8}{9}$   |
| 4   | $\pm \sqrt{\frac{1}{7} \left( 3 - 2\sqrt{\frac{6}{5}} \right)}; \pm \sqrt{\frac{1}{7} \left( 3 + 2\sqrt{\frac{6}{5}} \right)}$ | $\frac{1}{2} + \frac{\sqrt{30}}{36}; \frac{1}{2} - \frac{\sqrt{30}}{36}$ |

Table 2. LOW-ORDER GAUSS-LEGENDRE QUADRATURE WEIGHT-COEFFICIENTS



ACTUALLY  
SHIMA  
TERMS  
ATION SPHEROID  
CONCLUDES  
Paragraphize  
parallel

INCUBATED  
EXPOSED  
GEOCENTRIC  
SERIES  
FINDING  
WEINTRIT  
parameters  
DETERMINED  
DISTANCE  
RELATIVE  
Spec.  
FUKUSHIMA  
meridian  
ubiquitous  
ORTHODROMIC  
ISHELZKY

Copyright 2012

tagxedo.com







Copyright 2012

[tagxedo.com](http://tagxedo.com)

# SOLSTICE: An Electronic Journal of Geography and Mathematics

Persistent URL:  
<http://deepblue.lib.umich.edu/handle/2027.42/58219>



Deep Blue



IMaGe Home



Solstice Home



Institute of Mathematical Geography. All rights reserved in all formats.

Works best with a high speed internet connection.

Final version of IMaGe logo created by Allen K. Philbrick from original artwork from the Founder.

## VOLUME XXIII, NUMBER 2; December, 2012

### Part 2. Geosocial Networking: A Case from Ann Arbor, Michigan

David E. Arlinghaus and Sandra L. Arlinghaus  
Associated .kmz download.





lands adjacent to a creek, environmentally-sensitive residents quite naturally became concerned for the trees and wildlife that will be destroyed or disturbed. The project is still on-going and the geosocial network described below remains in place.

The County coded its easement with pink flags. It tagged selected large trees or otherwise interesting vegetation with a blue band if they were to be removed; it tagged trees within the easement with a red band if they were to be left alone. All vegetation within the easement, except trees or shrubs carrying red tags, were to be removed. Color was critical—a simple red/blue confusion could cost a tree its life!

One neighborhood used Google Earth, together with a GPS-enabled smartphone, to make an inventory of trees present, along a half-mile stretch of the creek, before the project began. David E. Arlinghaus did all the photography with a smartphone that geotagged the images. He then transmitted the images to Sandra L. Arlinghaus who did the mapping using a combination of GeoSetter and Google Earth (Figure 1).

Follow up in July of 2012, following the removal of trees and stream bank stabilization enabled the neighborhood to continue to track the progress of the project. Figures 2 through 8 show a sequence of screen captures from the field photographs. Figures 2 through 6 show the successes and failures (related to a drought) of larger, staked plantings. Figures 7 and 8 shows two of the many stream bank photos designed to illustrate the broader vegetation restoration.

Captions reveal some of what can be noted; however, to get a full view, download the linked .kmz file at the top of this article and open it in Google Earth. In that way, the reader of this article can follow along with what is happening in this territory without having to walk through the somewhat difficult terrain! Follow where the county is spending tax payer dollars on an important environmental restoration project!



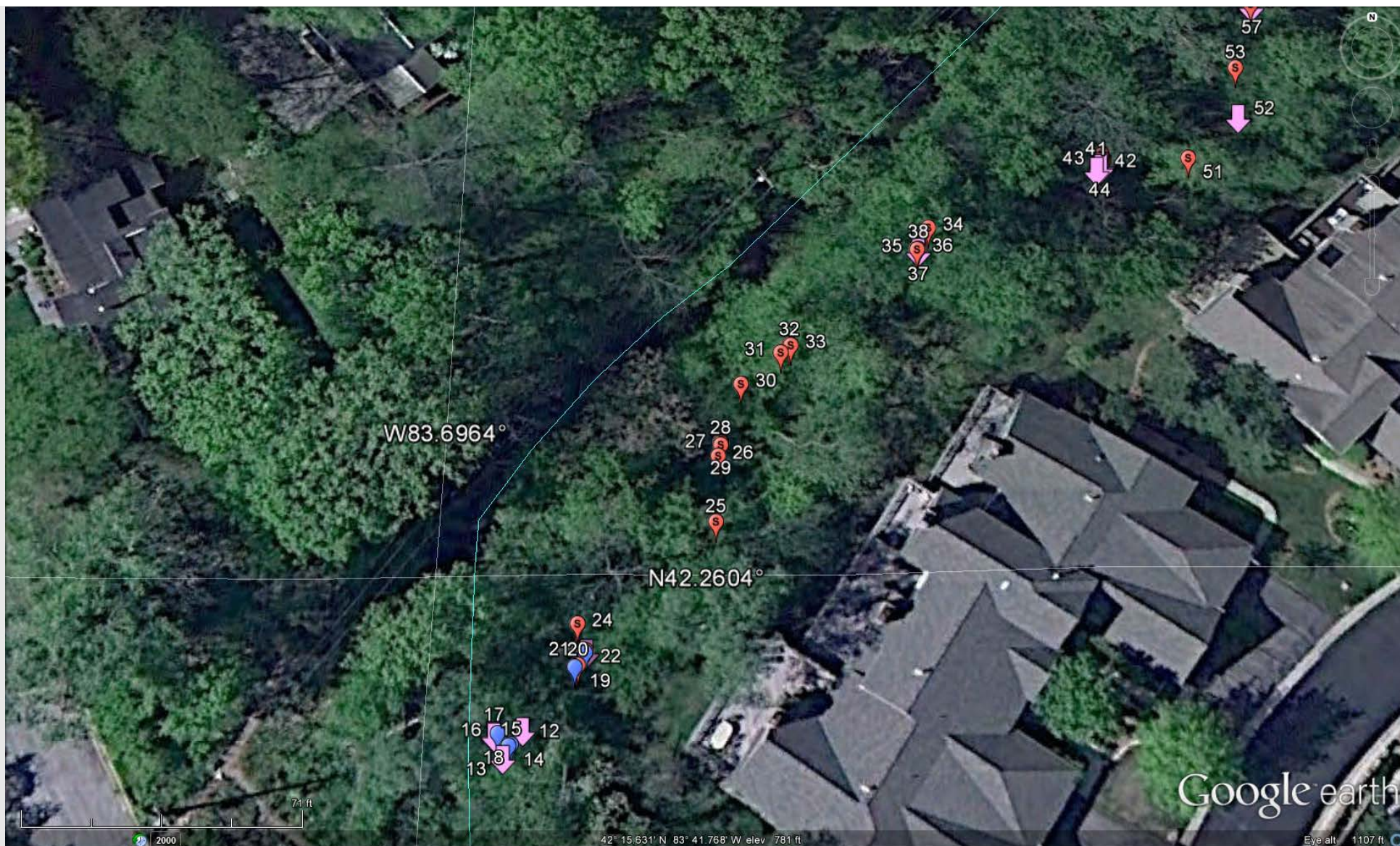


Figure 1. The original survey, prior to stream bank restoration. Pink arrows mark flags showing County drain easements. Red balloons mark trees to be saved within the easement. Blue balloons mark trees to be cut.

The accuracy of the geotagging of the photos was limited by several factors. First, the software in the smartphone has limits. Second, the geotagging of the tree is actually the geotagging of the camera where David stood to take the picture of the tree, rather than of the tree position, itself. He attempted to stand at a consistent distance from trees to ensure precision (but that is difficult in this terrain). The level of precision, however, was quite good—trees were in correct relation to each other and in close to correct relation to dwelling units.

The geotagged camera images were downloaded directly to a computer by plugging the smartphone into a recent Windows 7 desktop computer. The 191 images were stored in a single folder. That folder was then uploaded to the free software called "GeoSetter." From there, the geotagged images were batch-uploaded to Google Earth in a single operation (rather than entering each one individually). The GeoSetter software was able to take the underlying geocoded coordinates from the camera images, as well as the images



themselves, and make them correspond to the underlying coordinate geometry in Google Earth. We made color decisions to correspond with the actual colors of tags used on vegetation.

Accuracy, of registration of photo and Google Earth coordinates, using this sort of strategy was guaranteed. Hand placement would not offer that level of accuracy of registration. Overall, the results were sufficiently precise (although not accurate) to offer local residents a clear picture of what did happen in their local wooded areas.

When the camera GPS coordinates were obtained, a photo of the tagged item was also taken. The figures below show the photo pointing to a location. These pointing associations are all accurate.

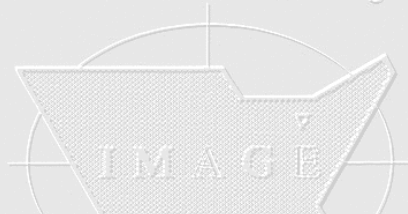
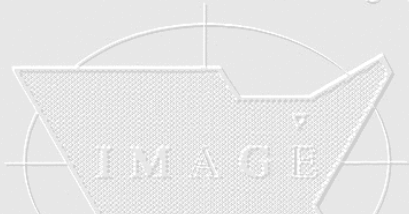


Figure 2. A large number of new trees were planted; these plants were larger than shrubs but not huge trees. They needed to be staked but could easily be planted with a shovel.





Figure 3. The staked trees were planted in an area not serviced by the condominium association sprinkler system; this image shows clearly the effects of the drought in early summer of 2012 (through much of July).





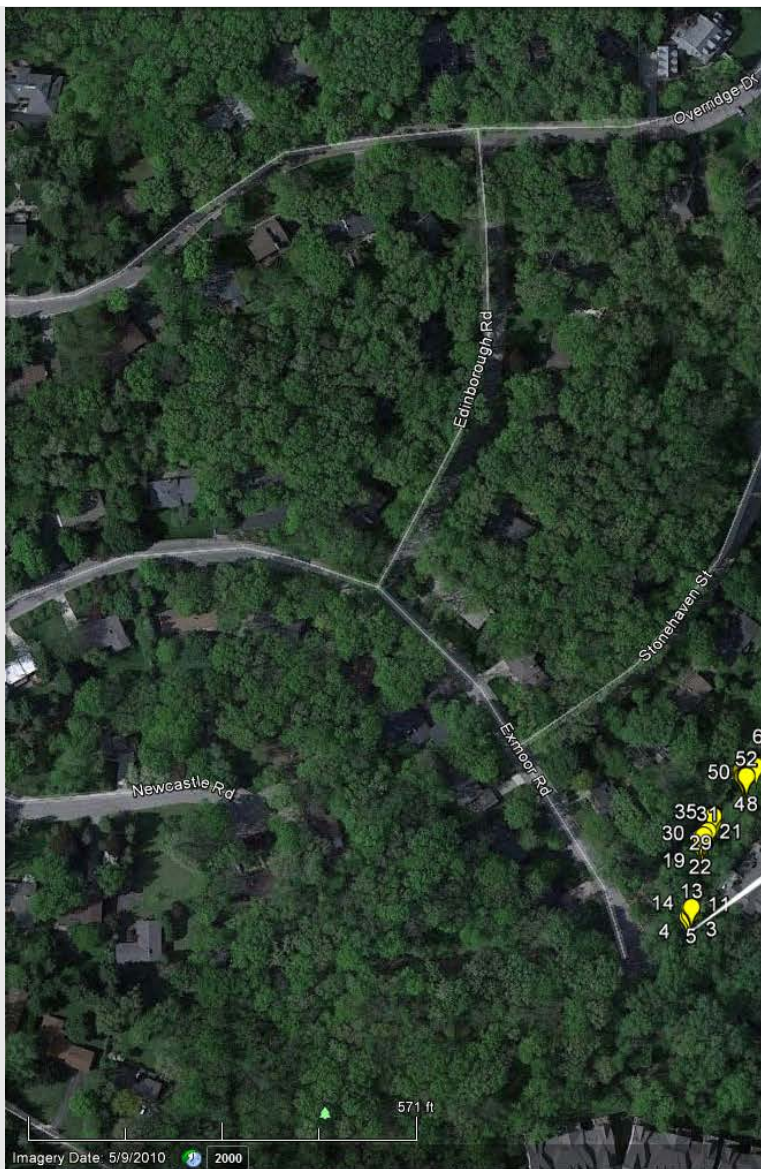


Figure 4. Some new trees did well, thanks to individual attention from local residents.

Institute of Mathematical Geography

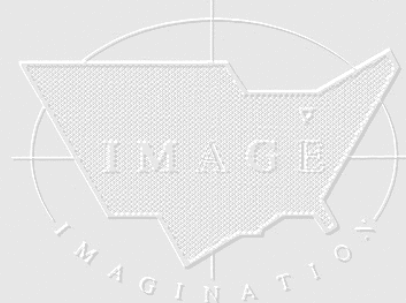
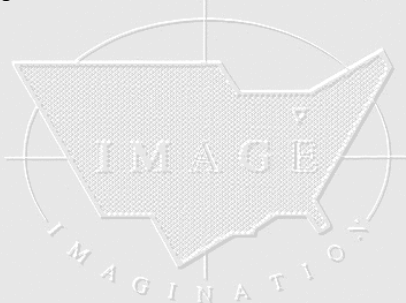
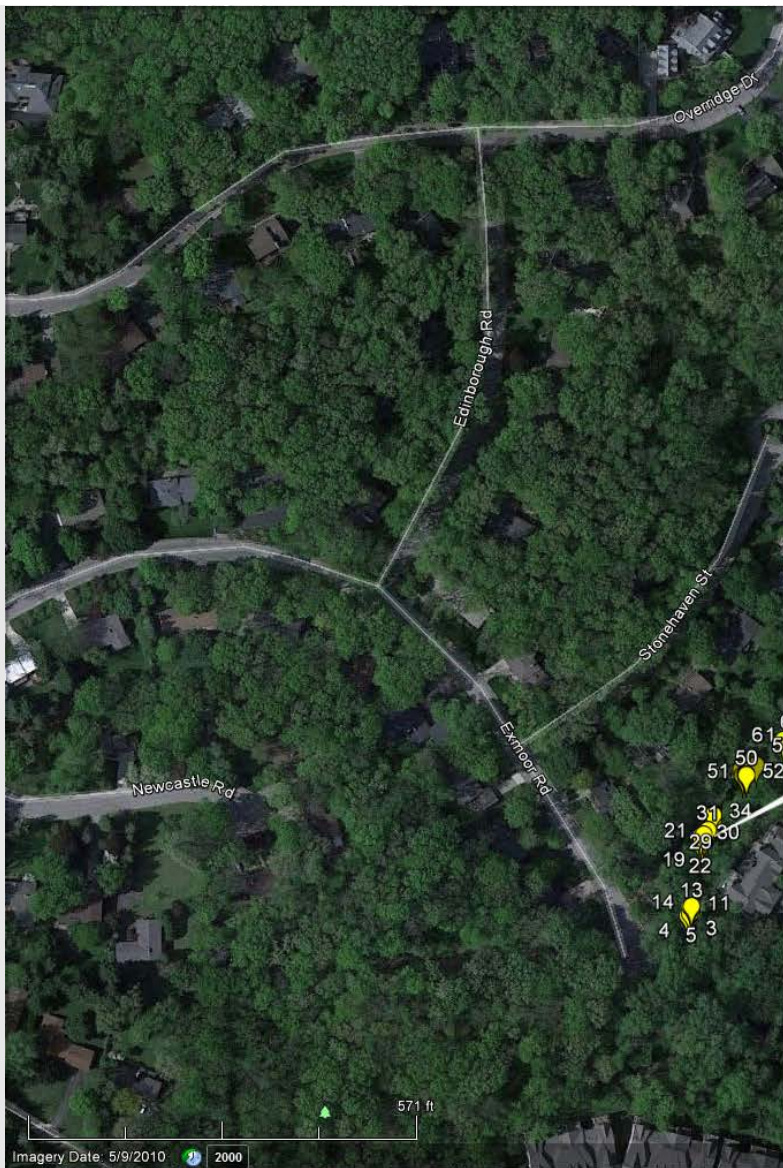
Institute of Mathematical Geography

Institute of Mathematical Geography

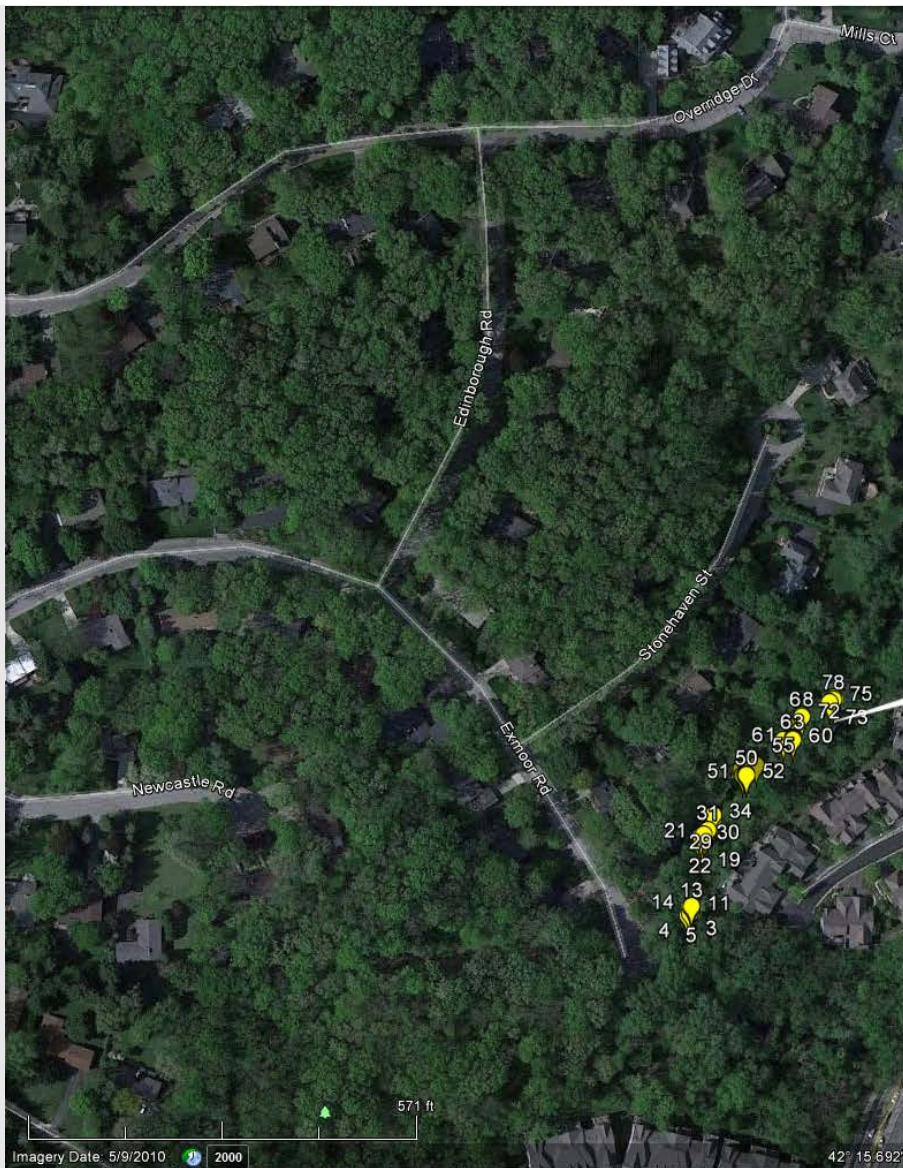
Institute of











78

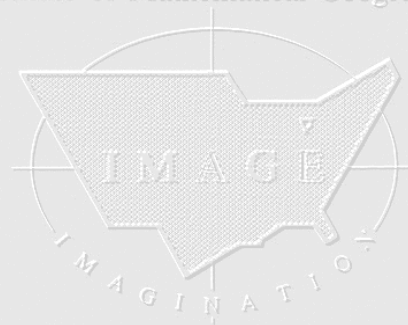
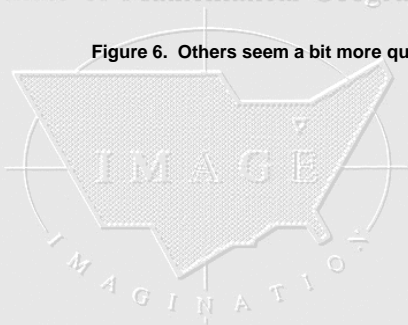


IMG\_20120714\_160628

Taken Date: 7/14/2012 4:06:27 PM  
Coordinates: N42°15'39.51", W83°41'43.74"  
Model: VM670  
Rating: 0  
File Size: 2206739  
File Date: 7/14/2012 4:06:28 PM



Figure 6. Others seem a bit more questionable...





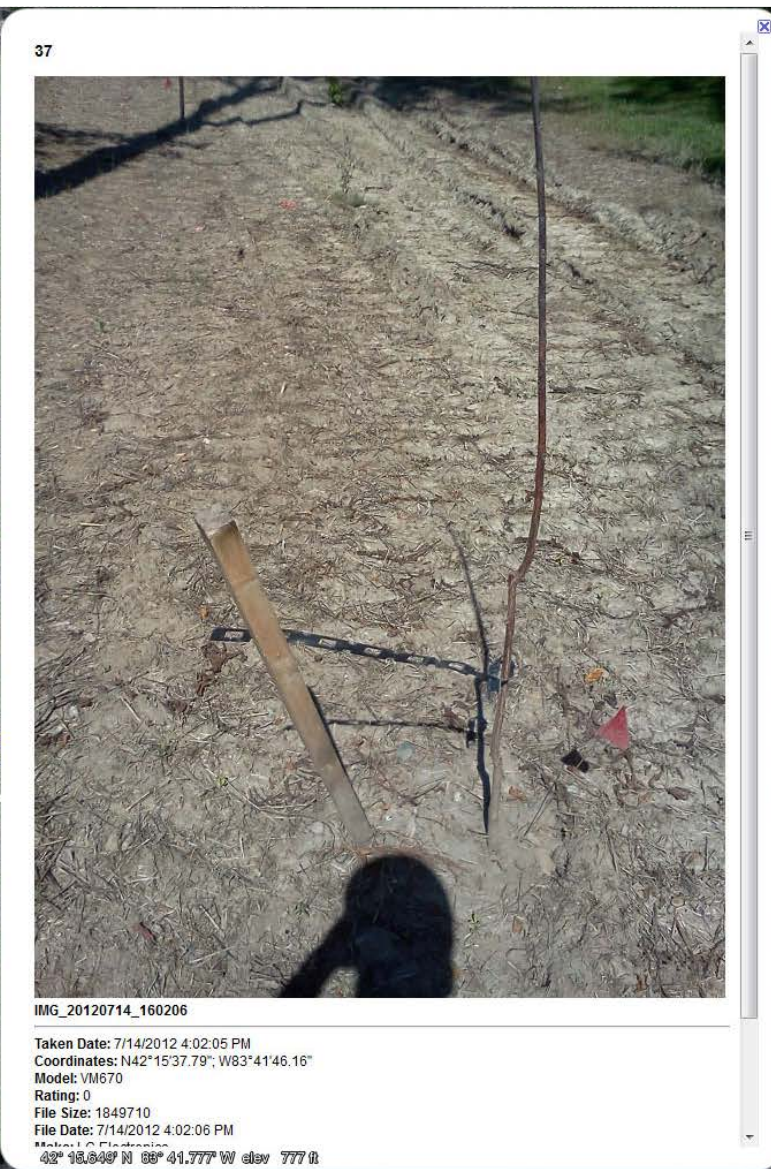
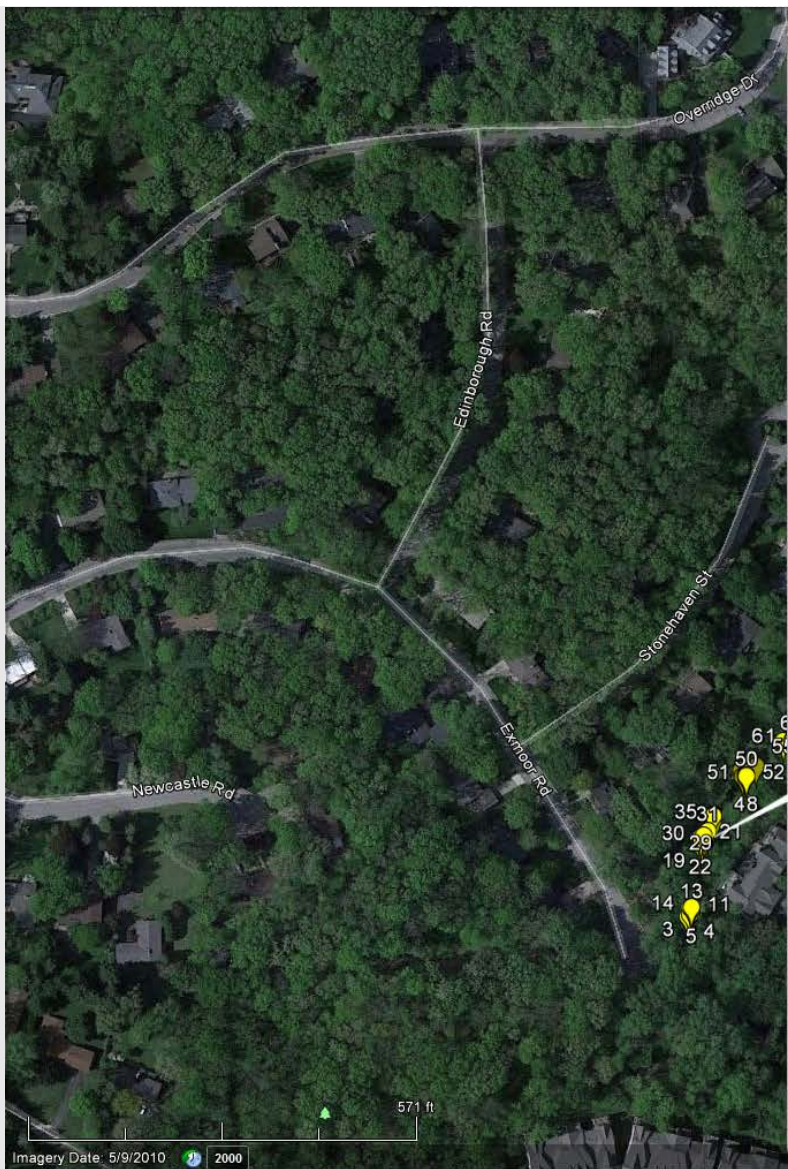


Figure 7. And then there were none? Trees like this one will apparently be replaced during the spring of 2013.





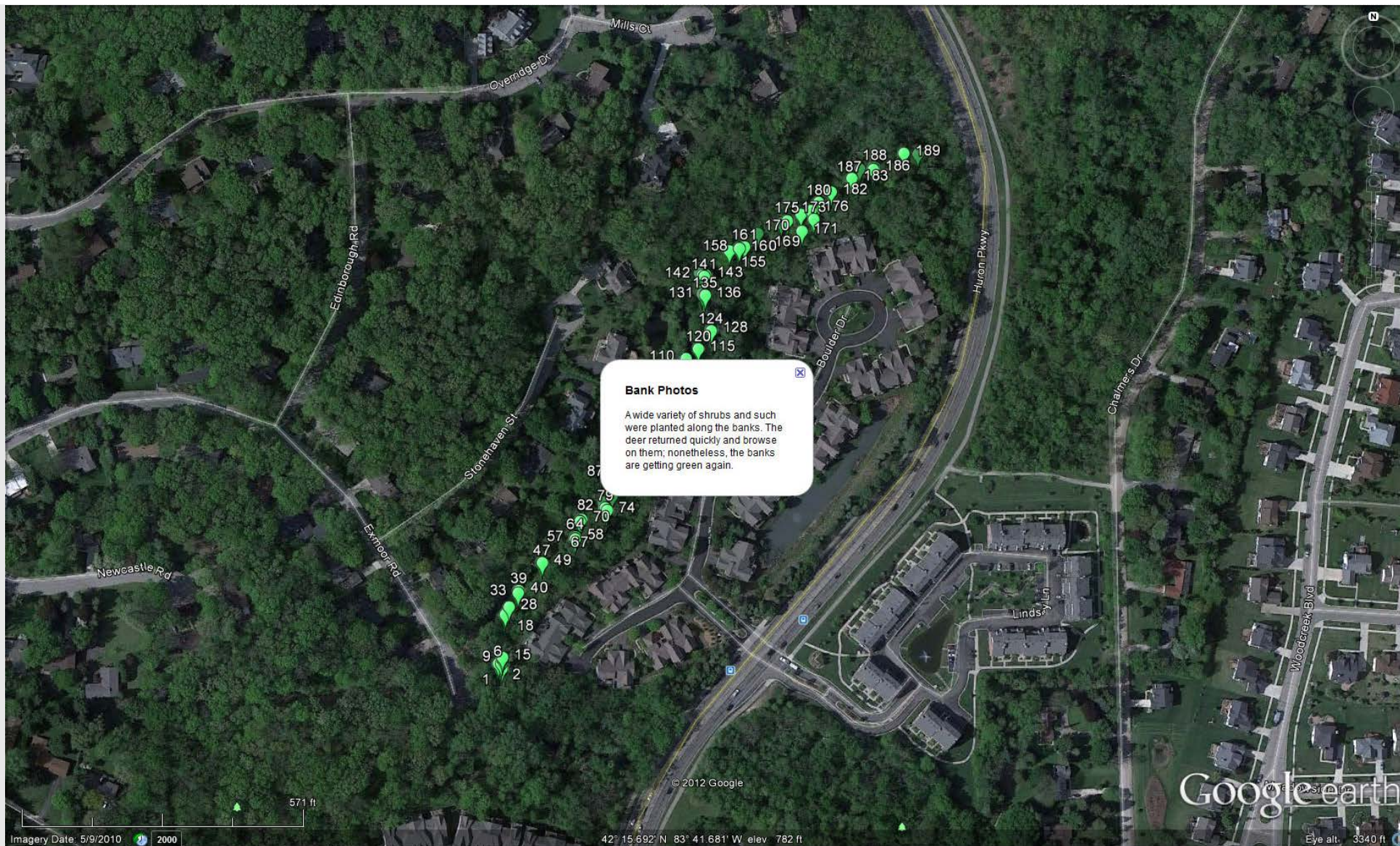


Figure 8. Distribution of photos of generalized bank vegetation.



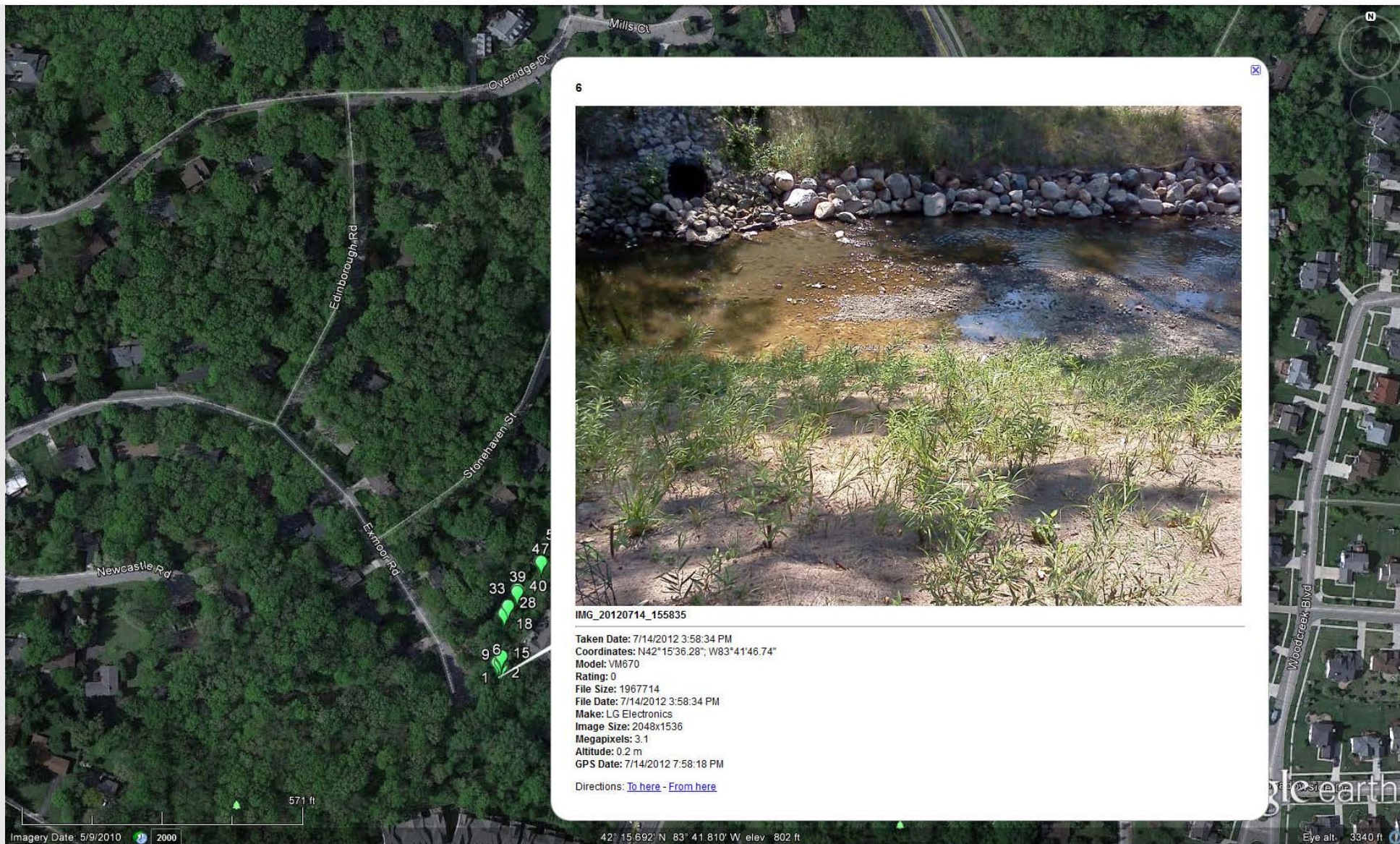
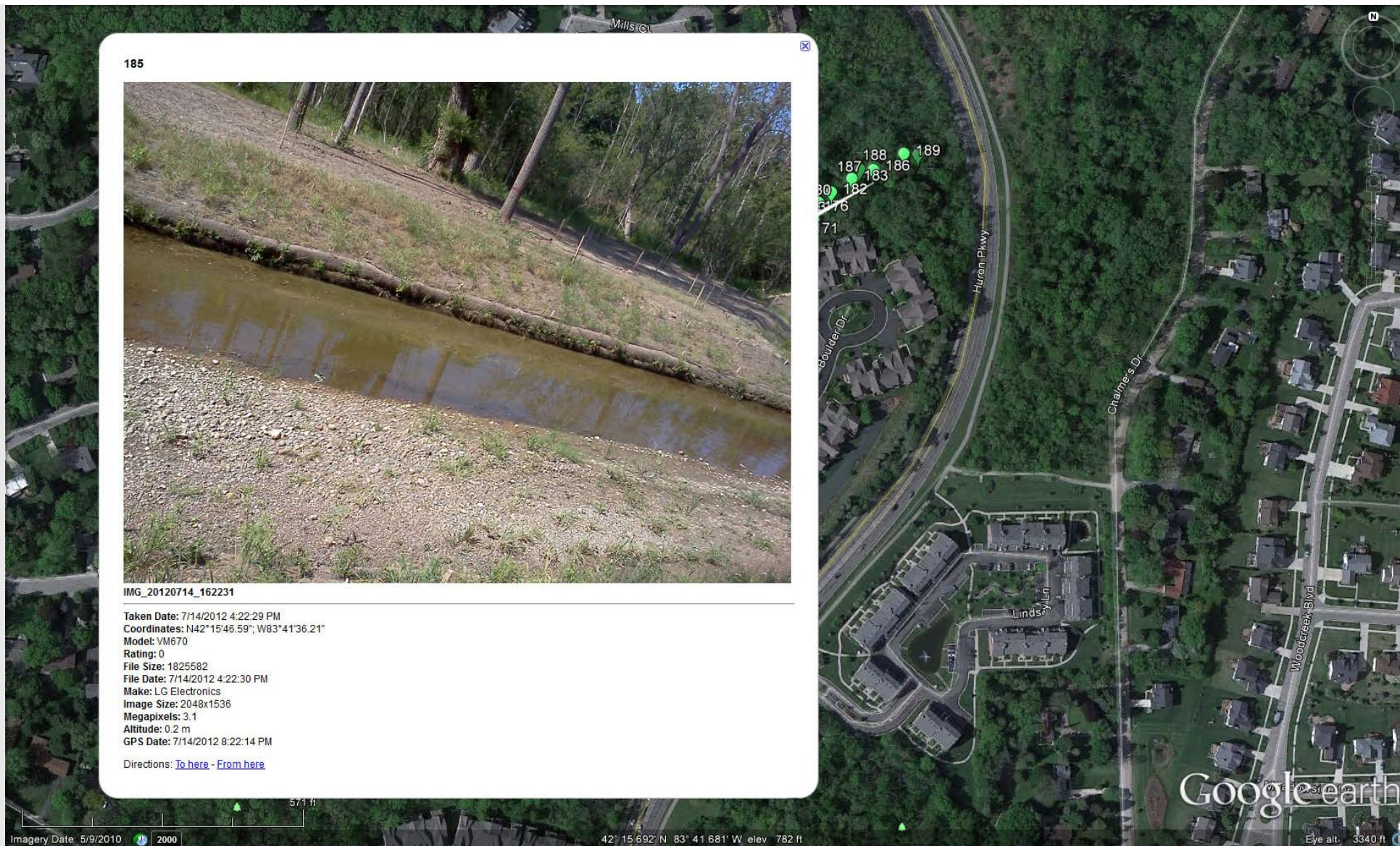


Figure 9. The bank appears to be filling in nicely with a mix of vegetation planted early enough to benefit from rains prior to the drought and to watering by persistent residents during the drought.





185



IMG\_20120714\_162231

Taken Date: 7/14/2012 4:22:29 PM  
 Coordinates: N42°15'46.59", W83°41'36.21"  
 Model: VM670  
 Rating: 0  
 File Size: 1825582  
 File Date: 7/14/2012 4:22:30 PM  
 Make: LG Electronics  
 Image Size: 2048x1536  
 Megapixels: 3.1  
 Altitude: 0.2 m  
 GPS Date: 7/14/2012 8:22:14 PM

Directions: [To here](#) - [From here](#)

Imagery Date: 5/9/2010 2000

42° 15' 692" N 83° 41' 681" W elev. 782 ft

Eye alt. 3340 ft

Figure 10. In other locations, the banks did not fare as well...the locational characteristics prevented supplemental watering. Still, by the end of July, some plants survive...will that survival rate be sufficient to cover the bank? Stay tuned...

The neighborhood association established a tree monitoring committee. The committee was given a Google Earth file showing tree location and associated tag color. The easement was also geocoded. Prior to using the file, the neighborhood association president and the creator of the Google Earth display met with the lead County official and the lead engineer on the project to ensure a cooperative approach to file usage. Subsequently, the tree monitoring committee used the information in conjunction with field-checking vegetation. Geosocial networking was, and is (through remaining tree restoration scheduled in spring 2013), critical in developing a constructive relationship among the various parties adjacent to this well-meant and successful environmental stream-bank restoration project.

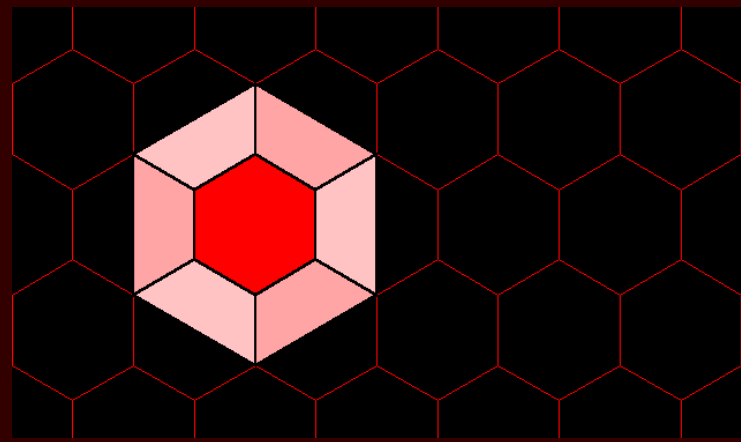
**References**



- Friedemann Schmidt. **GeoSetter**. Last accessed June 15, 2012: <http://www.geosetter.de/en/>
- Geosocial Networking, **Wikipedia**. Last accessed June 15, 2012: [http://en.wikipedia.org/wiki/Geosocial\\_networking](http://en.wikipedia.org/wiki/Geosocial_networking)
- **Google Earth**. Last accessed June 15, 2012: <http://www.google.com/earth/index.html>
- **Washtenaw County. Mallett's Creek Restoration Project: Final Report**. Last accessed June 15, 2012: [http://www.ewashtenaw.org/government/drain\\_commissioner/dc\\_webWaterQuality/malletts\\_creek/dc\\_mc\\_mcrp.html](http://www.ewashtenaw.org/government/drain_commissioner/dc_webWaterQuality/malletts_creek/dc_mc_mcrp.html)

**Acknowledgements**

Numerous people were involved directly and indirectly in this project that brought together County and City officials, Engineers from a local engineering firm, and members of the public from a variety of neighborhoods including differing residential types and zoning. We thank: Harry Sheehan, Greg Marker, Jane Lumm, Roger Rayle, Janice Bobrin, Matt Naud, and all the member neighborhoods of the [Huron Valley Neighborhood Alliance](#) and the individuals from those neighborhoods who participated in so many helpful ways.



**1. ARCHIVE**

**2. Editorial Board, Advice to Authors, Mission Statement**

**3. Awards**

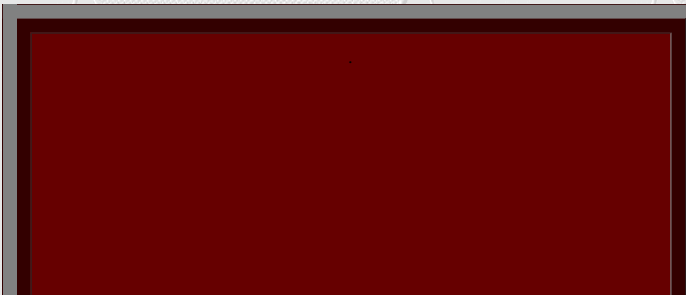
1.



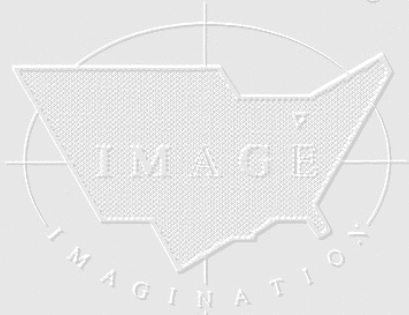
2.



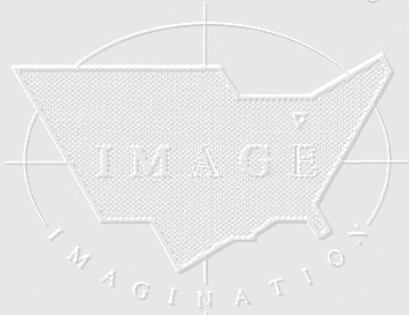
3.



Institute of Mathematical Geography



Institute of Mathematical Geography

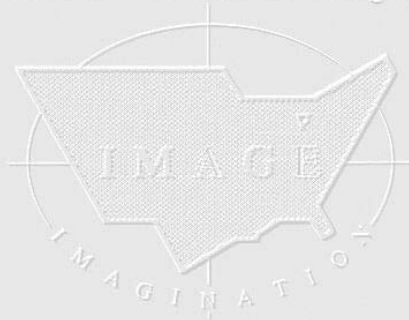


Institute of Mathematical Geography



1964 Boulder Drive,  
Ann Arbor, MI 48104  
734.975.0246  
<http://deepblue.lib.umich.edu/handle/2027.42/58219>  
[sarhaus@umich.edu](mailto:sarhaus@umich.edu)

Institute of Mathematical Geography



*Solstice*: An Electronic Journal of Geography and Mathematics,  
Institute of Mathematical Geography (IMaGe).  
All rights reserved worldwide, by IMaGe and by the authors.  
Please contact an appropriate party concerning citation of this article:  
[sarhaus@umich.edu](mailto:sarhaus@umich.edu)  
<http://www.imagenet.org>  
<http://deepblue.lib.umich.edu/handle/2027.42/58219>

*Solstice* was a **Pirelli** INTERNETional Award Semi-Finalist, 2001 (top 80 out of over 1000 entries worldwide)

One article in *Solstice* was a **Pirelli** INTERNETional Award Semi-Finalist, 2003 (Spatial Synthesis Sampler).

*Solstice* is listed in the **Directory of Open Access Journals** maintained by the University of Lund where it is maintained as a "searchable" journal.

*Solstice* is listed on the journals section of the website of the American Mathematical Society, <http://www.ams.org/>

*Solstice* is listed in **Geoscience e-Journals**

IMaGe is listed on the website of the Numerical Cartography Lab of The Ohio State University: [http://ncl.sbs.ohio-state.edu/4\\_homes.html](http://ncl.sbs.ohio-state.edu/4_homes.html)

Congratulations to all *Solstice* contributors.

Remembering those who are gone now but who contributed in various ways to *Solstice* or to IMaGe projects, directly or indirectly, during the first 25 years of IMaGe:

Allen K. Philbrick | Donald F. Lach | Frank Harary | William D. Drake |  
H. S. M. Coxeter | Saunders Mac Lane | Chauncy D. Harris | Norton S.  
Ginsburg | Sylvia L. Thrupp | Arthur L. Loeb | George Kish |

A way to look at geographical movement:

In this note movement is considered between geographical places identified by geographical coordinates of the beginning and ending locations. This movement may consist of a single person (or other entity: an idea, artifact, commodity, etc.) or multiple persons. The path taken is not considered and the movement takes place during some specified time interval. The assumption is made that there may be many moves, from dozens to millions.

The pair of locations, as point locations can be rendered as one directed line (arrow), as between points on a map, and the entire group of movements as many arrows. An example is shown in the first illustration: Journey to Work in the Detroit vicinity. All this is well known. It is also conventional, when many movements are involved, to group beginning and ending locations into aggregated locations: separate little pieces of territory. These are often counties, census tracts, states or countries, etc., irregularly shaped polygons on the earth's surface. The movement between these areas can be shown in a similar manner to that of point location data, generally using area centroids. This is shown in the next figure, having made using the Flow Mapper program from CSISS.org.

What I would like to suggest now is that one may imagine shrinking these areal units into small size, really infinitesimally small, and then to consider the movement pattern in a spatially continuous fashion. This can be done by introducing a grid, or raster, over the domain and reassigning all of the movements to the nodes in this grid. This is accomplished by smoothly spreading all of the movement from (or to) an area over the nodes bounded by each of the movement reporting areas. Such a raster covering the contiguous United States is illustrated here.

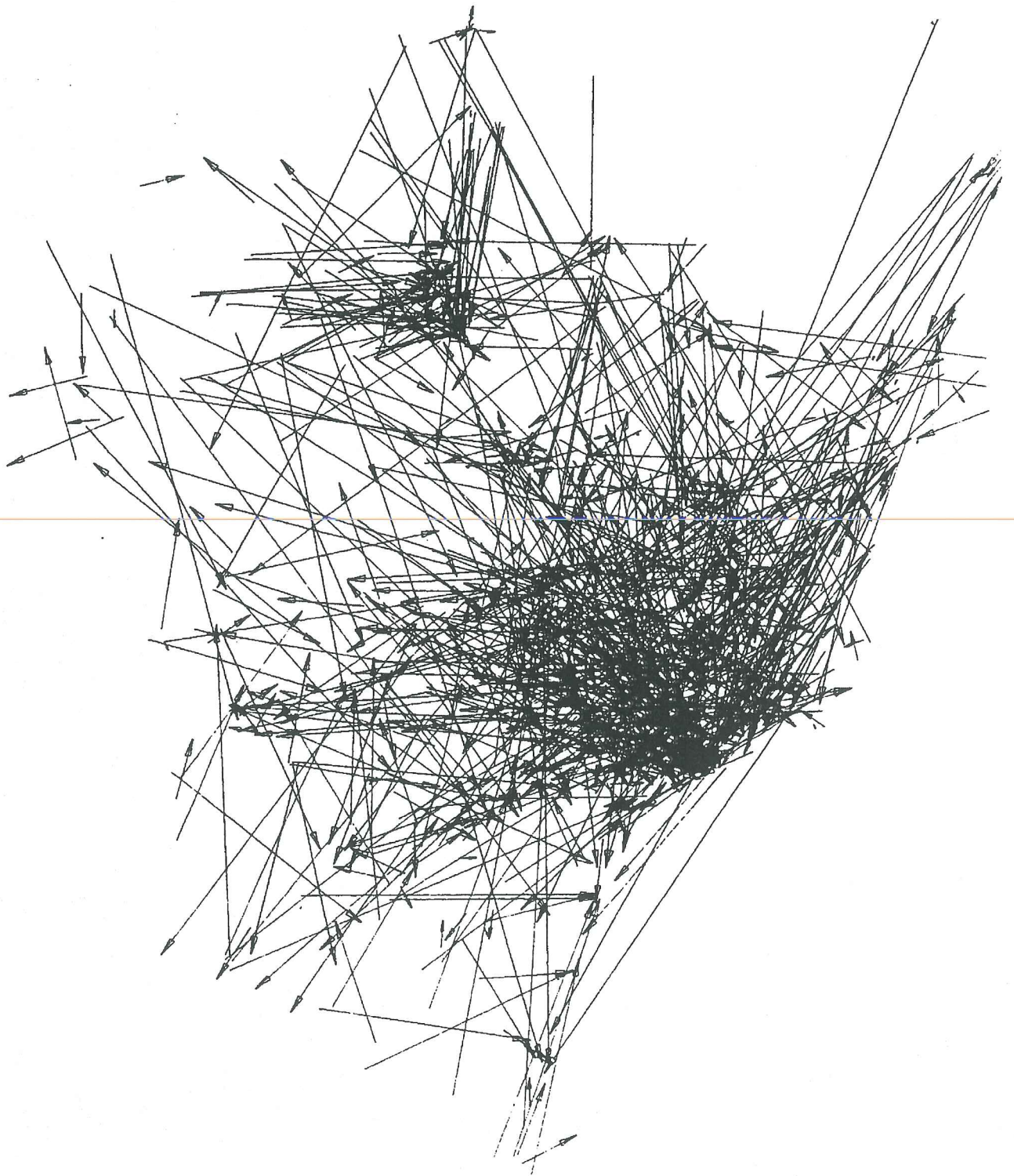
A suggested next step is to consider the difference between the incoming and outgoing moves within each area, in the raster assignment. Thus some of the areas (i.e., raster nodes) will get positive numbers and some will have negative numbers. Imagine that the negative numbers are high hills and the positive numbers represent low valleys - i.e., you have a kind of topographic surface. Now let the movement quantities move downhill, like topography eroding. The movement arrows are now the gradients to the "movement surface", and can be shown as a vector field. Connecting these gradient vectors can render this as a streamline movement pattern.

The example shows these ideas using a U.S. Census Bureau 48 by 48 contiguous state-to-state migration table converted in this fashion. The hills are the out-migration quantities and the low places, e.g., Florida, are the in-migration places. The resulting movement pattern clearly delineates source and sink domains describing the net spatial pattern of migration. In this particular depiction sixteen million people are migrating: the trajectories are ensemble averages, not individual moves. But migration to the Northwest, Southwest, Southeast, and Northeast are clearly distinguished. That this migration map resembles a map of wind or ocean currents is not surprising given that we speak of migration "flows" and "backwaters" and use many such hydrodynamic terms when discussing migration and movement phenomena. The appearance is that of laminar flow, due in part to the coarse resolution of the data.

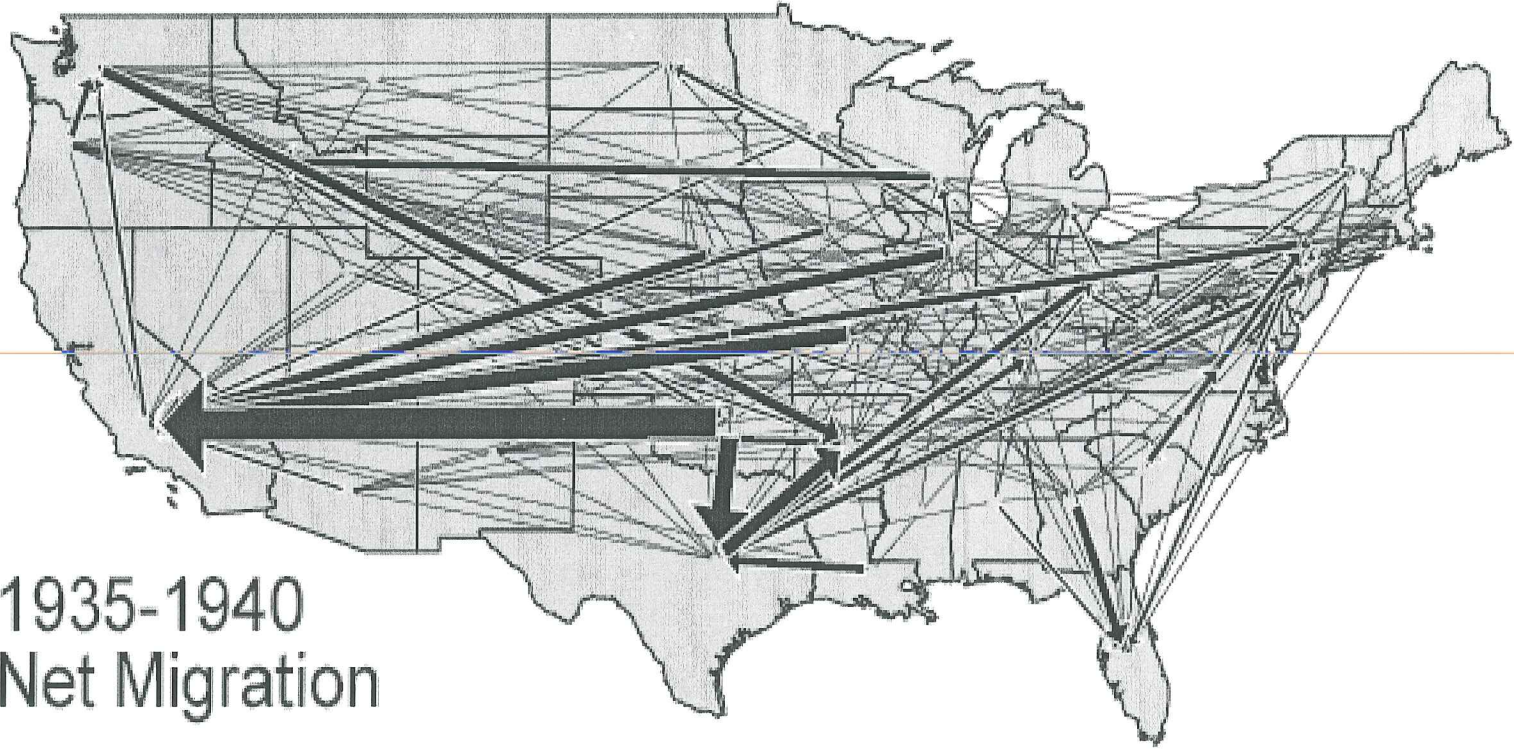
The suggestion is that this continuous type of movement pattern analysis can be used in other situations, such as movement within a city, perhaps based on data assembled from cellular phone observations when connected to GPS locations. Many other such situations come to mind. For example, taxes collected and entitlements disbursed, both by congressional district.

Waldo Tobler  
<http://www.geog.ucsb.edu>

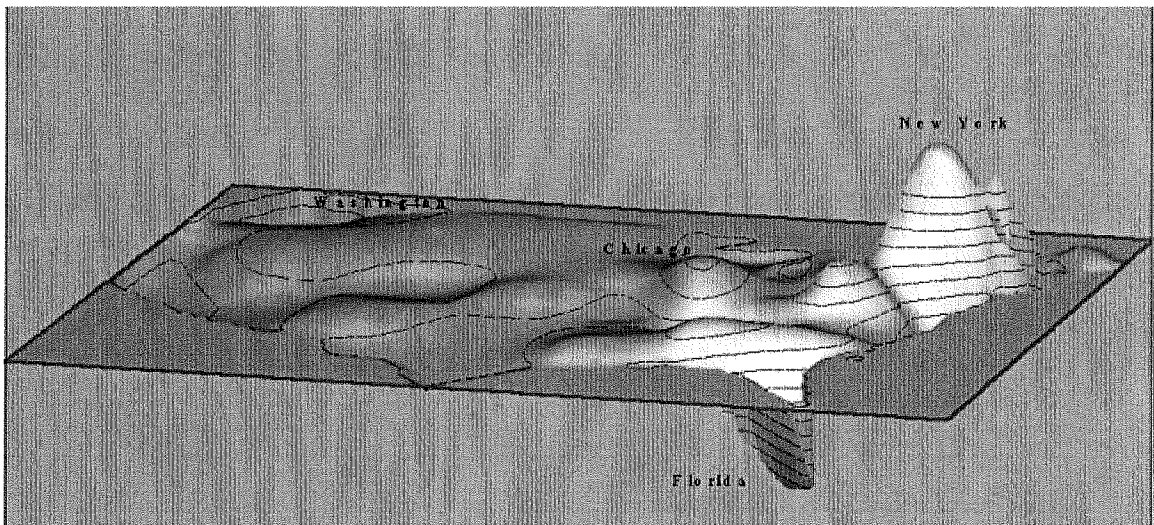


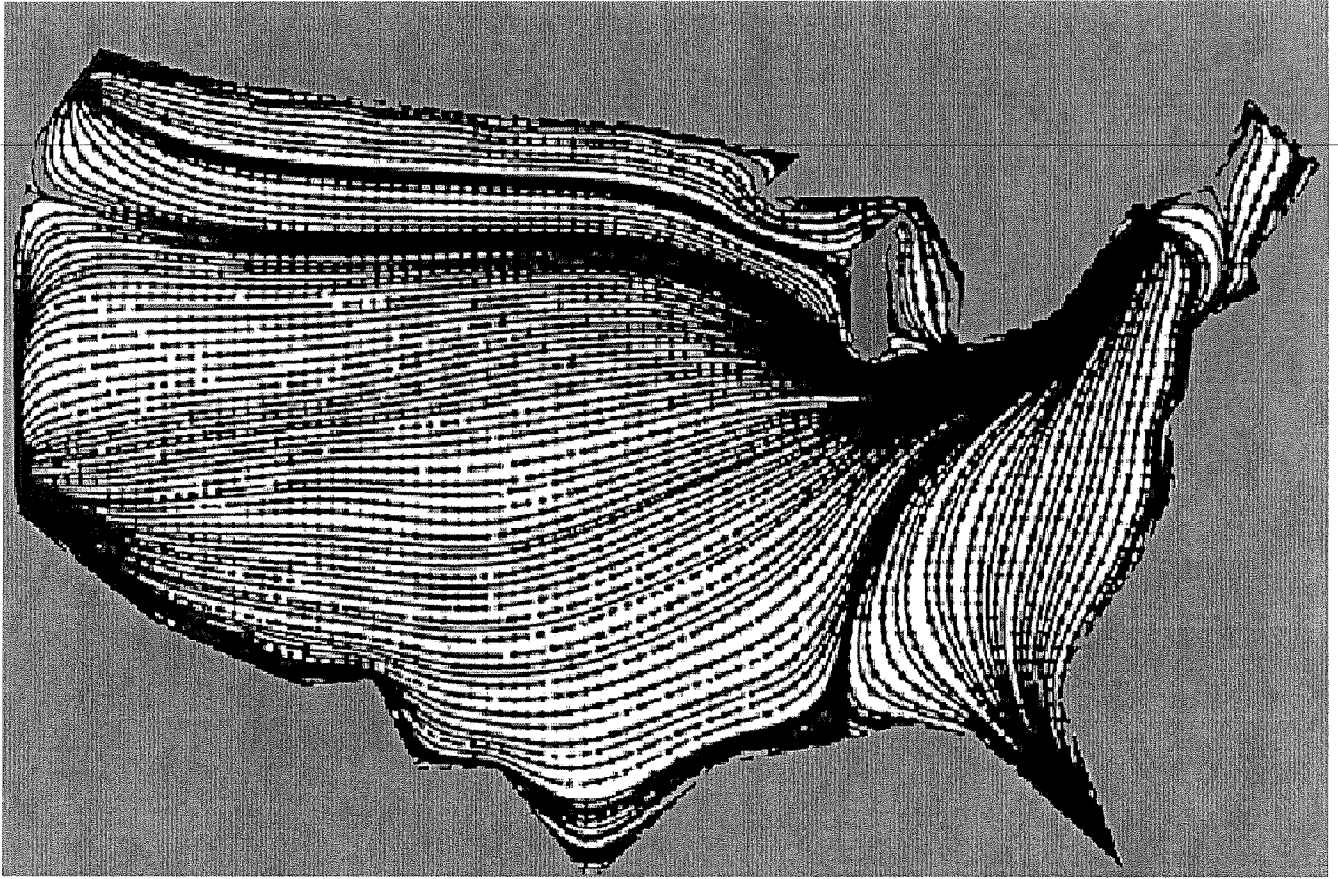






1935-1940  
Net Migration







# SOLSTICE: An Electronic Journal of Geography and Mathematics

Persistent URL:

<http://deepblue.lib.umich.edu/handle/2027.42/58219>



Deep Blue



IMaGe Home



Solstice Home



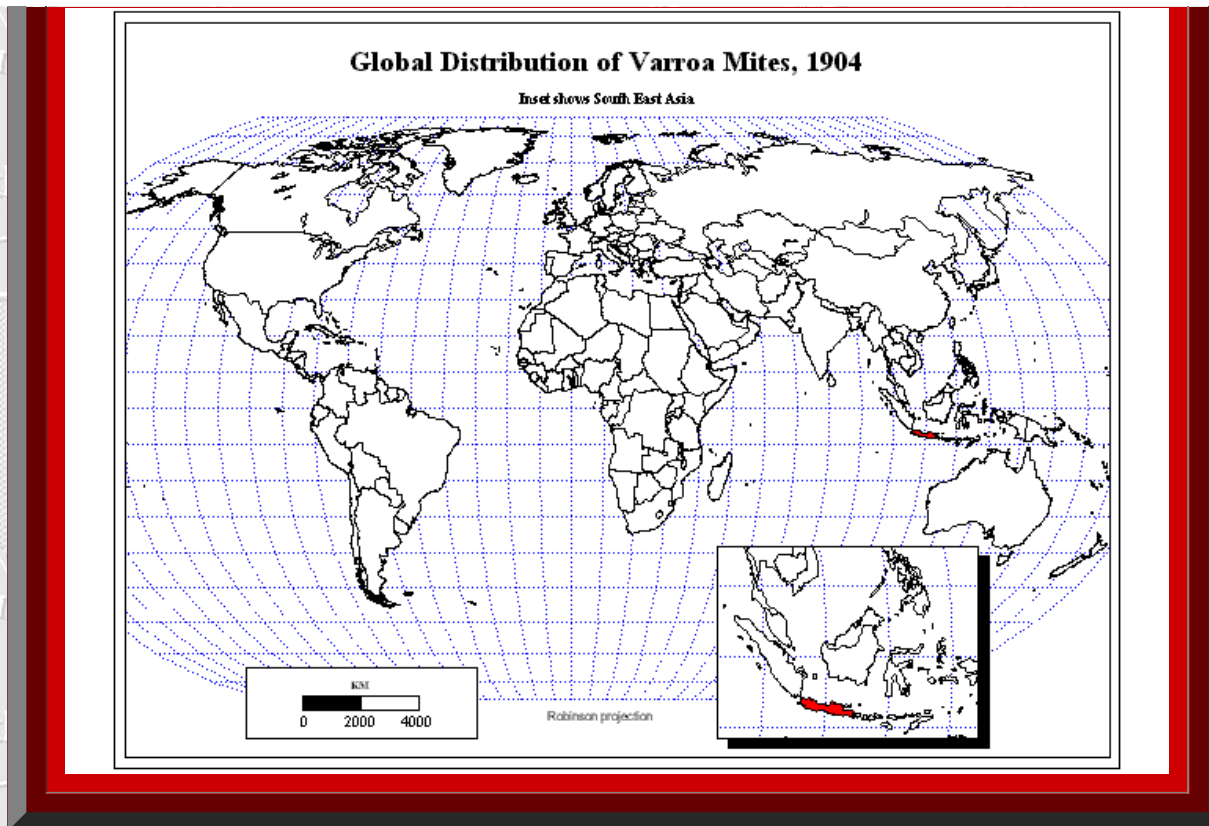
Institute of Mathematical Geography, All rights reserved in all formats.  
Works best with a high speed internet connection.

Final version of IMAge logo created by Allen K. Philbrick from original artwork from the Founder.

## Update on Varroa Mite Spread

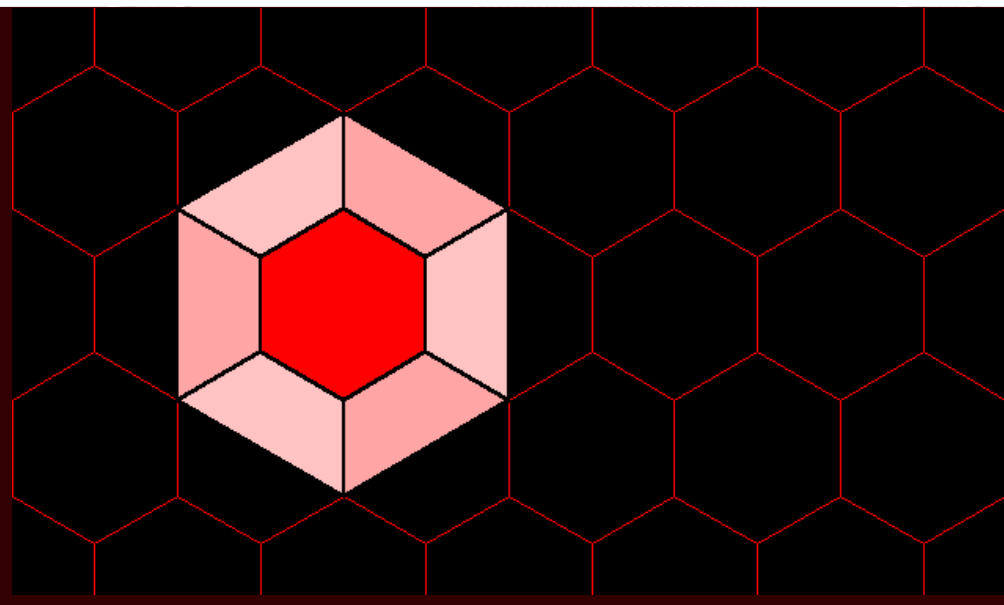
Diana Sammataro





- **Nigeria has been added to the list of impacted countries.** Akinwande, K.L. , Badejo, M.A., Ogbogu, S.S. Incidence of the Korean haplotype of Varroa destructor in southwest Nigeria ( Short Survey ) *Journal of Apicultural Research*, Volume 51, Issue 4, 1 October 2012, Pages 369-370.
- **Hawaii, part of the Big Island and all of Oahu are now impacted.** Martin, S.J., Highfield, A.C., Brettell, L., Villalobos, E.M., Budge, G.E., Powell, M., Nikaido, S., Schroeder, D.C. 2012. Global honey bee viral landscape altered by a parasitic mite. *Science*. 336 (6086): 1304-1306 <http://www.sciencemag.org/content/336/6086/1304.abstract>
- **Current work with the Swiss Bee Research Center is ongoing to map and update Varroa spread.**  
**Stay tuned for more information and for updates of the animated Varroa mite mapping project.**





**1. ARCHIVE**

**2. Editorial Board, Advice to Authors, Mission Statement**

**3. Awards**

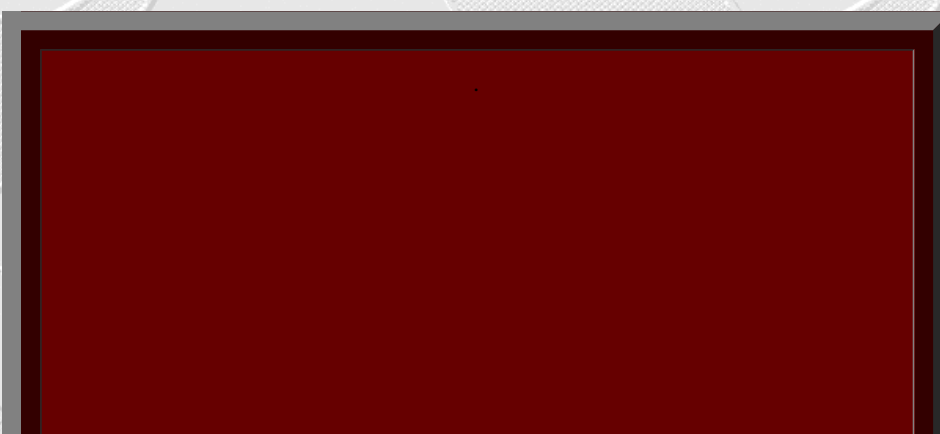
1.



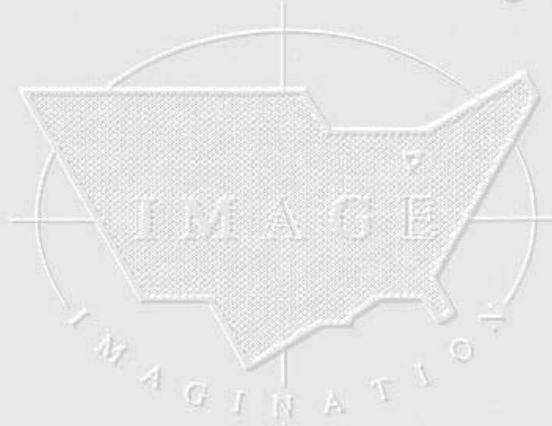
2.



3.



## Institute of Mathematical Geography



*Solstice: An Electronic Journal of Geography and Mathematics*,  
Institute of Mathematical Geography (IMaGe).

All rights reserved worldwide, by IMaGe and by the authors.  
Please contact an appropriate party concerning citation of this article:

[sarhaus@umich.edu](mailto:sarhaus@umich.edu)

<http://www.imagenet.org>

<http://deepblue.lib.umich.edu/handle/2027.42/58219>

*Solstice* was a Pirelli INTERNETional Award Semi-Finalist, 2001 (top 80 out of over 1000 entries worldwide)

One article in *Solstice* was a Pirelli INTERNETional Award Semi-Finalist, 2003 (Spatial Synthesis Sampler).

*Solstice* is listed in the [Directory of Open Access Journals](#) maintained by the University of Lund where it is maintained as a "searchable" journal.

*Solstice* is listed on the journals section of the website of the American Mathematical Society, <http://www.ams.org/>

*Solstice* is listed in [Geoscience e-Journals](#)

IMaGe is listed on the website of the Numerical Cartography Lab of The Ohio State University: [http://ncl.sbs.ohio-state.edu/4\\_homes.html](http://ncl.sbs.ohio-state.edu/4_homes.html)

---

Congratulations to all *Solstice* contributors.

Remembering those who are gone now but who contributed in various ways to *Solstice* or to IMaGe projects, directly or indirectly,



during the first 25 years of IMAge:

Allen K. Philbrick | Donald F. Lach | Frank Harary | William D. Drake |  
H. S. M. Coxeter | Saunders Mac Lane | Chauncy D. Harris | Norton S.  
Ginsburg | Sylvia L. Thrupp | Arthur L. Loeb | George Kish |

1964 Boulder Drive,  
Ann Arbor, MI 48104  
734.975.0246

<http://deepblue.lib.umich.edu/handle/2027.42/58219>  
[sarhaus@umich.edu](mailto:sarhaus@umich.edu)





DIRECT GEOGRAPHICAL MAP LINKAGE  
ORIGINAL SUBGROUP USES QUESTIONS UNDERSTANDING  
WORLDS horizontal equivalent ANALOGY SMARTPHONE RESULT

Copyright 2012

[tagxedo.com](http://tagxedo.com)

# **SOLSTICE:** **An Electronic Journal of Geography and Mathematics**

Persistent URL:

<http://deepblue.lib.umich.edu/handle/2027.42/58219>



Deep Blue



IMaGe Home



Solstice Home



Institute of Mathematical Geography, All rights reserved in all formats.

Works best with a high speed internet connection.

Final version of IMAge logo created by Allen K. Philbrick from original artwork from the Founder.

## **VOLUME XXIII, NUMBER 2; December, 2012**

### **QR Code Transformations**

Sandra L. Arlinghaus





Copyright 2012

tagxedo.com

Map transformation is an idea that is familiar to most geographers (Tobler, 1961; Thompson, 1917; Coxeter, 1961). A QR code might be viewed as a "map"---it employs a mathematical code to direct understanding of content. While the geographical map uses mathematics to guide understanding of content of the Earth, the QR code map uses mathematics to guide understanding within electronic worlds ([link to general pattern of meaning within a QR code](#)).

One might ask questions about QR codes in the same way one does about geographical maps. Not all regions of a map carry equal weight (land masses on one map might be more important than water masses). The same observation is true about QR codes--different regions of the image carry different weights (as indicated in material in the link above). The thoughtful reader will think of numerous parallels. Is there some sort of parallel world of QR-cartography?

### Geometric Transformations

Rotation (turn), reflection (flip), and translation (slide) form a basic set of movements of figures in the plane (Coxeter, 1961). In the case of a QR code pattern in a box, it is clear that translation does not affect the code--simply slide the smartphone to catch up with the sliding motion of the QR code box. Do rotation and reflection of the surface pattern in the box alter the linkage to a website? Does the embedded link to a website get destroyed by such motion? If not, does the link remain constant under such transformation. Again, it seems clear that if the link is not destroyed that then the rotated or reflected QR code would point to the same url as the original QR code box....it is simply the surface pattern and not the embedded code that is being transformed. Figure 1 shows a single QR code that has had transformations applied to it. Figure 1a is the "original" pattern. Figure 1b shows the pattern with a horizontal flip. Figure 1c shows the pattern with a vertical flip. Figure 1d shows it rotated 45 degrees clockwise.



Figure 1a. Base QR code. Links to IMaGe home site.



Figure 1b. Horizontal flip of Figure 1a.



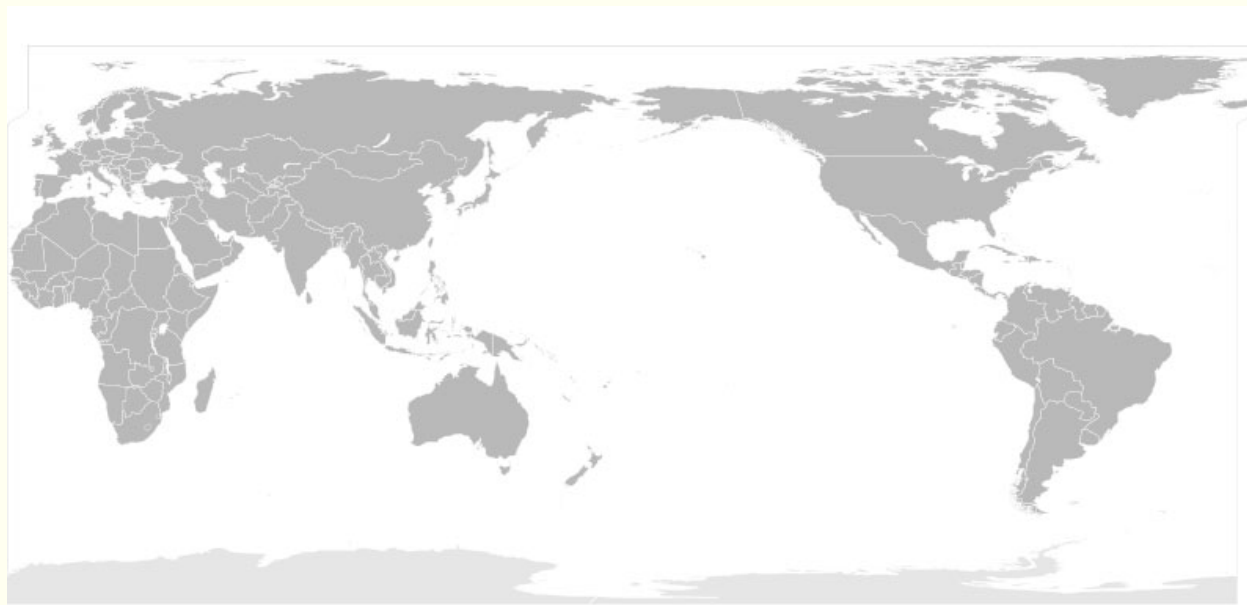
Figure 1c. Vertical flip of Figure 1a.



Figure 1d. Rotation of Figure 1a through 45 degrees clockwise.

This simple experiment suggests that rotation does not destroy the linkage of the pattern to a website but that reflection does do so. At first, this result might seem surprising. If, however, one returns to the analogy of QR codes and geographic maps, it might not. The difference is that QR code patterns are not sensible to our eye whereas many map patterns are. Thus, in the sequence of maps in Figures

2a through 2d, it makes sense that the original and the rotated map (Figures 2a and 2d) are equivalent in terms of content but that the flipped maps in Figures 2b and 2c are not sensible in that regard. Nonetheless, QR codes such as the flipped ones that are not sensible from an overhead view might become useful in situations where one wishes to look at the QR code from the back or from underneath. The animation in Figure 2c shows the distinction between rotating the map through 180 degrees (so that north and south are interchanged) and reflecting, or flipping, the map.



**Figure 2a.** Map of the world. Source: Public Domain, <http://en.wikipedia.org/wiki/File:BlankMap-World-162E-flat.svg>



**Figure 2b.** Horizontal reflection of the map in Figure 2a.



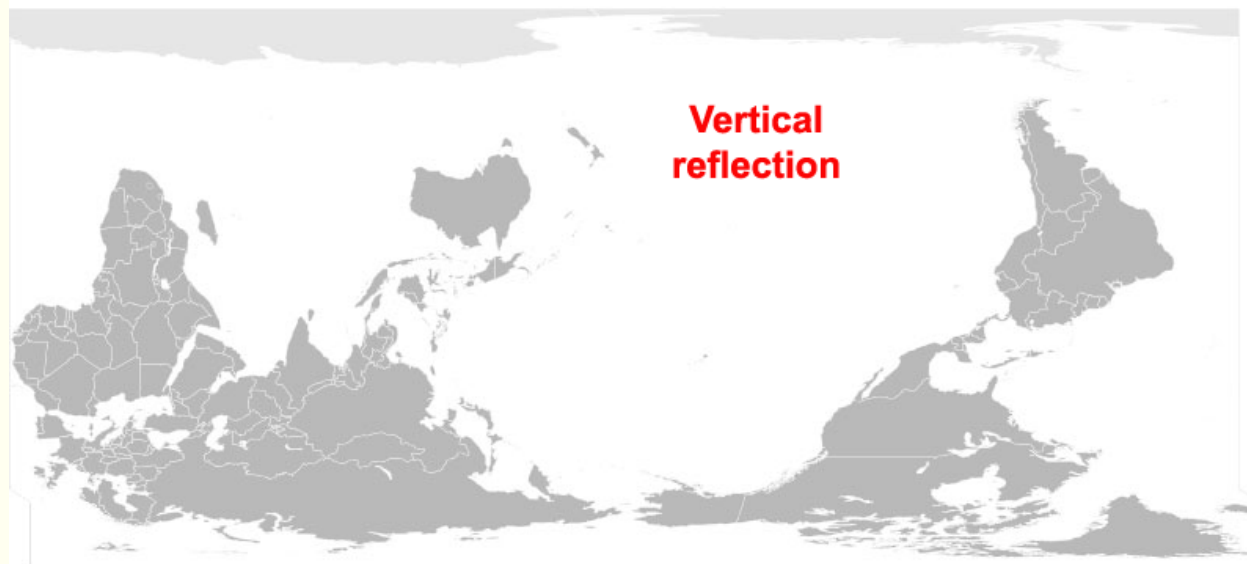


**Figure 2c.** Animation showing difference between a vertical reflection of the map in Figure 2a and a rotation through 180 degrees of the map in Figure 2a.



**Figure 2d.** Rotation through 45 degrees of the map in Figure 2a.

**If one looks further, at the interleaving of data and error correcting blocks that lie behind the QR code pattern, then one sees immediately-- due to lack of symmetry, that the Escher-like tiles of data are preserved under rotation but not under reflection (Figures 3a through 3d).**

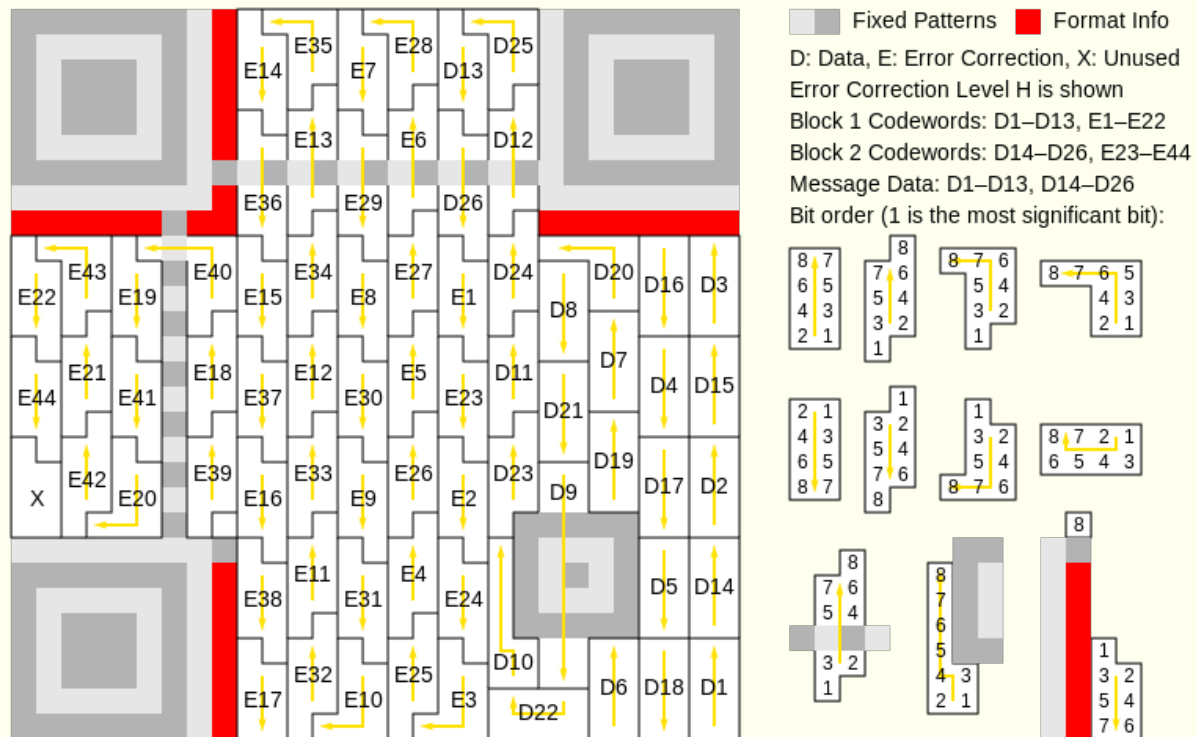


**Figure 3a.** Interleaving of tiles of data and error correction in tiles that change position under reflection but not under rotation.  
 Source: Public Domain, "Bobmath", *Wikipedia*, Jan. 9, 2012: [http://en.wikipedia.org/wiki/File:QR\\_Ver3\\_Codeword\\_Ordering.svg](http://en.wikipedia.org/wiki/File:QR_Ver3_Codeword_Ordering.svg)



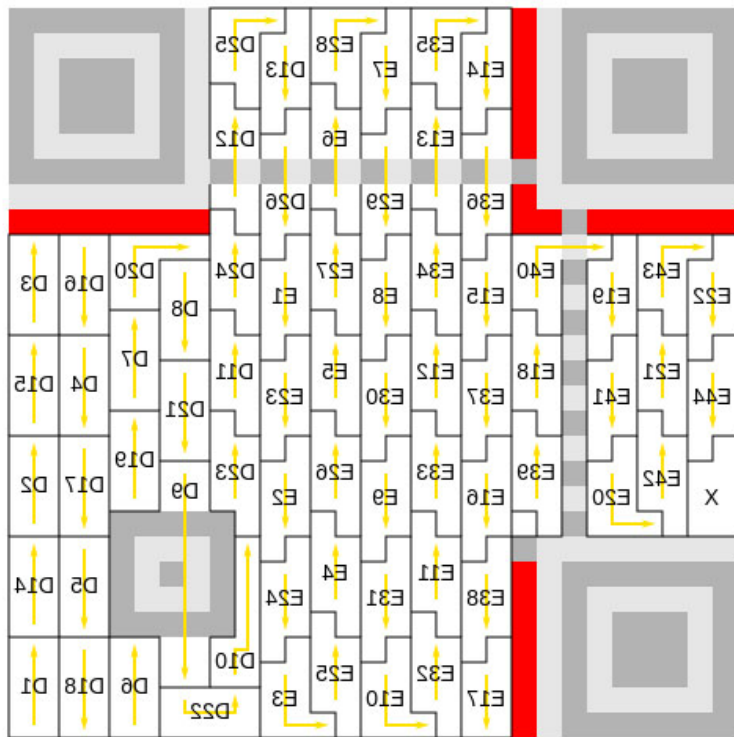


Figure 3b. Horizontal reflection alters relative interleaving of tiles.

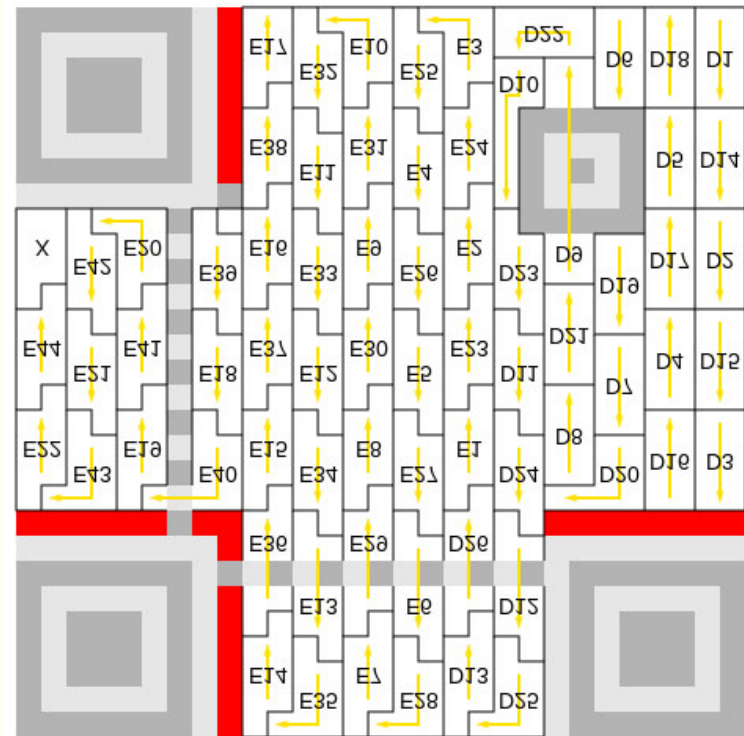


Figure 3c. Vertical reflection alters relative interleaving of tiles.

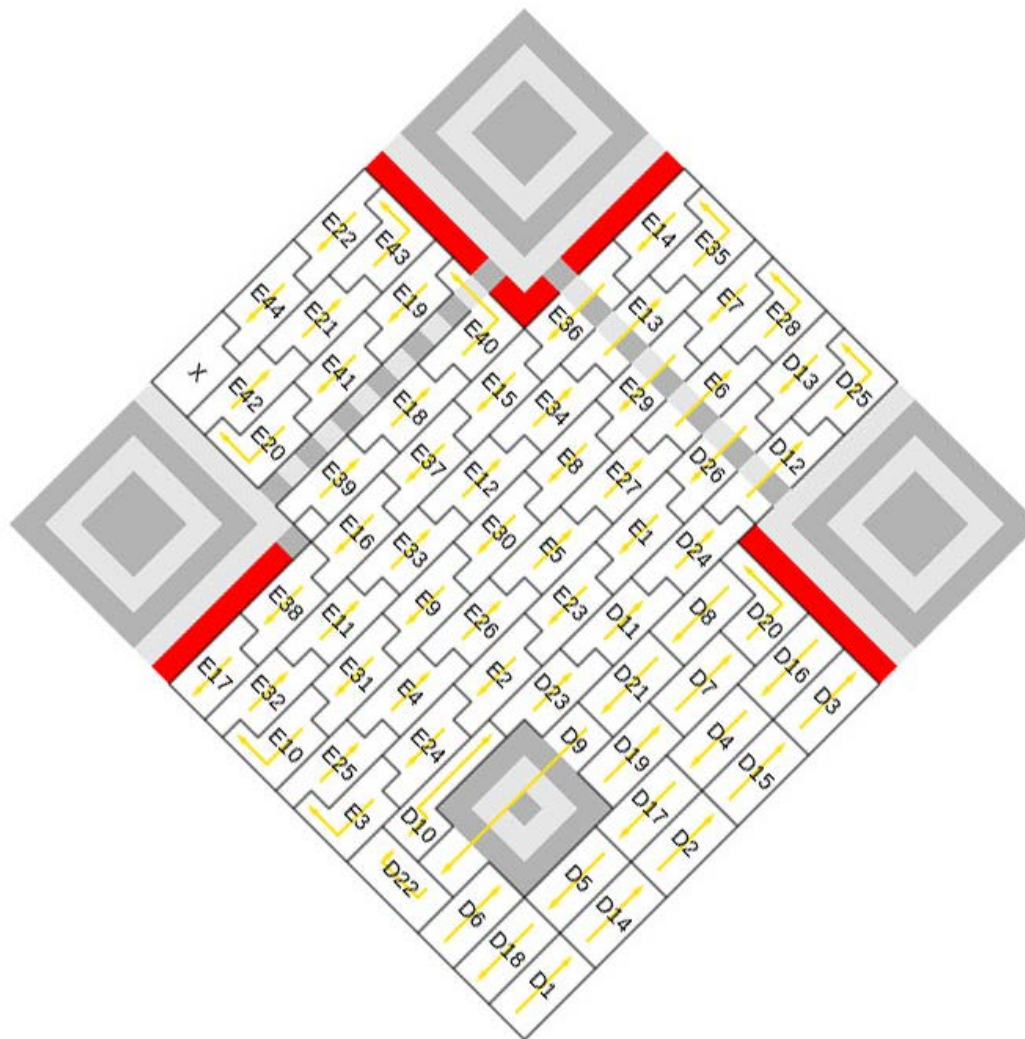


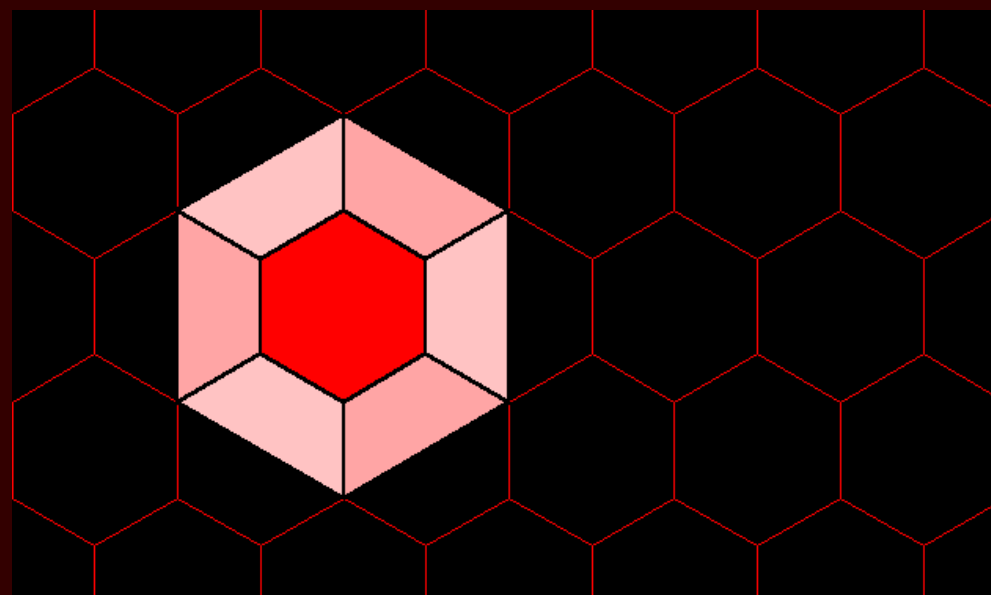
Figure 3d. Rotation through 45 degrees does not alter relative interleaving of tiles.

### Permutation Group of the Symmetries of a Square

Legal motions of a QR code form a subgroup of the group of motions of symmetries of a square. It is the subgroup of rotations. The QR code is invariant under the geometric transformations of rotation and translation, but not under reflection.

### References

- Coxeter, H. S. M. 1961. *Introduction to Geometry*. New York: John Wiley & Sons.
- Thompson, D'A. W. 1917. *On Growth and Form*. Cambridge University Press.
- Tobler, W. R. 1961. Map Transformations of Geographic Space. [Doctoral Dissertation](#).
- Wikipedia:
  - Bobmath. 2012, January 8. Codeword Ordering: [http://en.wikipedia.org/wiki/File:QR\\_Ver3\\_Codeword\\_Ordering.svg](http://en.wikipedia.org/wiki/File:QR_Ver3_Codeword_Ordering.svg) Last accessed, Nov. 23, 2012.
  - Lokal Profil. 2008, April 16. Blank Map World: <http://en.wikipedia.org/wiki/File:BlankMap-World-162E-flat.svg> Last accessed, Nov. 23, 2012.
  - QR code. [http://en.wikipedia.org/wiki/QR\\_code](http://en.wikipedia.org/wiki/QR_code) Last accessed, Nov. 23, 2012.
- Wolfram:
  - "[Group of Symmetries of the Square](#)" from [the Wolfram Demonstrations Project](#) <http://demonstrations.wolfram.com/GroupOfSymmetriesOfTheSquare/> Contributed by: [Enrique Zeleny](#) Last accessed, Nov. 23, 2012.
  - [Rowland, Todd](#) and [Weisstein, Eric W.](#) "Group." From [MathWorld](#)--A Wolfram Web Resource. <http://mathworld.wolfram.com/Group.html> Last accessed, Nov. 23, 2012.



### 1. ARCHIVE

2. Editorial Board, Advice to Authors, Mission Statement

### 3. Awards

1.

2.

3.





Institute of Mathematical Geography



***Solstice: An Electronic Journal of Geography and Mathematics,***  
**Institute of Mathematical Geography (IMaGe).**  
All rights reserved worldwide, by IMaGe and by the authors.  
Please contact an appropriate party concerning citation of this article:  
[sarhaus@umich.edu](mailto:sarhaus@umich.edu)  
<http://www.imagenet.org>  
<http://deepblue.lib.umich.edu/handle/2027.42/58219>

***Solstice* was a Pirelli INTERNETional Award Semi-Finalist, 2001 (top 80 out of over 1000 entries worldwide)**

**One article in *Solstice* was a Pirelli INTERNETional Award Semi-Finalist, 2003 (Spatial Synthesis Sampler).**

***Solstice* is listed in the Directory of Open Access Journals maintained by the University of Lund where it is maintained as a "searchable" journal.**

**Solstice** is listed on the journals section of the website of the American Mathematical Society, <http://www.ams.org/>

**Solstice** is listed in *Geoscience e-Journals*

IMaGe is listed on the website of the Numerical Cartography Lab of The Ohio State University: [http://ncl.sbs.ohio-state.edu/4\\_homes.html](http://ncl.sbs.ohio-state.edu/4_homes.html)

---

Congratulations to all *Solstice* contributors.

Remembering those who are gone now but who contributed in various ways to *Solstice* or to IMaGe projects, directly or indirectly, during the first 25 years of IMaGe:

**Allen K. Philbrick | Donald F. Lach | Frank Harary | William D. Drake | H. S. M. Coxeter | Saunders Mac Lane | Chauncy D. Harris | Norton S. Ginsburg | Sylvia L. Thrupp | Arthur L. Loeb | George Kish |**

1964 Boulder Drive,  
Ann Arbor, MI 48104  
734.975.0246

<http://deepblue.lib.umich.edu/handle/2027.42/58219>  
[sarhaus@umich.edu](mailto:sarhaus@umich.edu)







One might ask questions about QR codes in the same way one does about geographical maps. Indeed, is there some sort of parallel world of QR-cartography?

What alterations of a QR image do not destroy the embedded link to a website (or other)? Some of the answer to that question lies in the extent of embedded error correction within the underlying code. The greater the correction capability, the greater the surface pattern can be disrupted without loss of transmission capability. Nonetheless, are there certain geometric styles of pattern disruption that are permitted? Figure 1 shows simple pattern destruction that still permits code transmission.



Figure 1. Source: [http://en.wikipedia.org/wiki/File:QR\\_Code\\_Damaged.jpg](http://en.wikipedia.org/wiki/File:QR_Code_Damaged.jpg)

It is important to understand what sorts of alterations of QR code pattern will still permit decoding of the image. From an aesthetic viewpoint, it is important to be able to make attractive QR codes to encourage their use. From a marketing viewpoint, it is important to be able to make QR codes clearly linked to a business. And, from a municipal viewpoint, it is important to be able to make QR codes as parts of official documents that will withstand handling by multiple parties, as in the case of the recent adoption of a requirement by the City Council of the City of New York, that every city agency that has inspection, permit, license, or registration information online post a QR code linking to it (Pereira, 2012).

### Geometric Alterations within the Plane

#### Color Change

Perhaps the simplest alteration is color change. The contrast between dark and light needs to be sufficient for the scanner to make suitable distinctions, but beyond that, color is irrelevant. Black and white is no different from color. Changing color may slightly improve design appearance. As with a map, four colors suffice. Too many colors create visual clutter. The images in Figure 2 offer some ideas involving color change; all should decode by going to the same url. The interested reader can find any number of color (and other) variations created by folks all across the Internet: [link](#).





**Figure 2a.** QR code leading to IMAge home page.



**Figure 2b.** Image in Figure 2a with single color replacement.

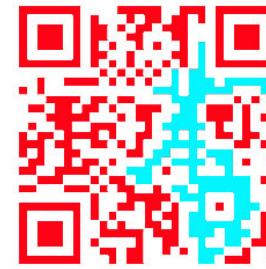


**Figure 2c.** Image in Figure 2a with more than single color replacement.

**Distortion**

Image creation software, such as Adobe Photoshop, may be used to soften the edges of images and introduce a host of filters. Some of these introduce distortion that is slight enough not to alter code transmission. The user is engaging in a balancing act with the level of error correction built into the code on one side and the level of power of image alteration on the other. Figure 3 offers a set of examples of image alteration through artistic distortion. Many others are available online ([Beautiful Pixels](#), 1010, for example). These distortions involve alteration of the pattern within a given canvas.



**Figure 3a.** Base figure worked with for much of this document.



**Figure 3b.** Straightforward use of several filters in Photoshop leaves the pattern clearly recognizable.



**Figure 3c.** Shearing the pattern creates an interesting effect. How much shearing is permitted?

More generally, one might wonder how the aspect ratio itself might be altered and still preserve code. Figure 4 offers a set of examples of image alteration through aspect ratio distortion (again, the level to which one can perform such distortion will be tied to error correction capability). In Figures 4a and 4b the decoding is swift. In Figure 4c, one scanner could not decode it while another could do so. Clearly there are limits to this sort of distortion but determining them is based on a variety of software, hardware, and error correction factors. What is important to note is that in fact there are limits beyond which aspect ratio distortion yields the code unusable. This fact might come into play if one were to consider tattoos on growing humans, etching QR codes into the bark of growing trees, and no doubt a variety of other possibilities involving a time or stretching of a surface factor.





Figure 4a. Based on Figure 3a: A 50% increase in height dimension while keeping width the same.



Figure 4b. Based on Figure 3a: A 70% increase in height dimension while keeping the width the same.



Figure 4c. Based on Figure 3a: An 80% increase in height dimension while keeping the width the same.

#### Interruption and Opacity

The shearing in Figure 3c interrupted the image (much as a cut in the ocean, as in a Goode's homolosine projection might interrupt a map). Screen savers often interrupt an image; in fact, that is the idea. Figure 5 shows an image of a QR code that remains readable despite being covered with a set of semi-opaque "bubbles" from a screen saver.



Figure 5. Bubble screen saver does not interrupt capability to decode pattern.

Figure 5 prompts questioning the extent to which one image may be slid (translated) across a QR code with opacity adjusted. Figure 6 shows a sequence of such codes. Again, the answer is a matter of balance. In Figure 6a, the hexagonal overlay is 100% opaque. The image does not scan. In Figure 6b, the overlay is 60% opaque and the image scans but it does not scan when set to 65%. In Figure 6c, the two overlays are set at 36% each. The image scans despite the opacity of the interior hexagon being greater than 36%. Clearly location of semi-opaque elements matters and leads to asking questions about where materials might be successfully embedded within a given QR code.



Figure 6a. Hexagon is 100% opaque.



Figure 6b. Hexagon is 60% opaque.



Figure 6c. Each hexagon is 36% opaque.

### Embedding

As translation is considered, what logos or other images in fully opaque form may be inserted within the QR code? The [linked](#) file explains the process. Figure 7 shows one existing example; there are many others.



Figure 7. QR code with embedded logo.

One can also turn the idea around and consider how to embed QR codes (altered or not) into existing art (as in Figures 8 and 9) or into art created with the QR code deliberately incorporated as an element of the art. A number of forward-looking original pieces of art, designed to have an embedded QR code are present in a variety of locales: one that seemed particularly attractive to this author were the examples present in the extensive PATH network linking underground downtown Toronto, Ontario locations.



**Figure 8.** Seurat, 1884. Pointillism. *A Sunday on La Grande Jatte*. Look for the QR code (from Figure 2a) embedded in Seurat's pointillist approach. There is sufficient contrast that most scanners should be able to decode the image, when viewed on a screen with high resolution, that has had the white background removed and replaced with transparency.



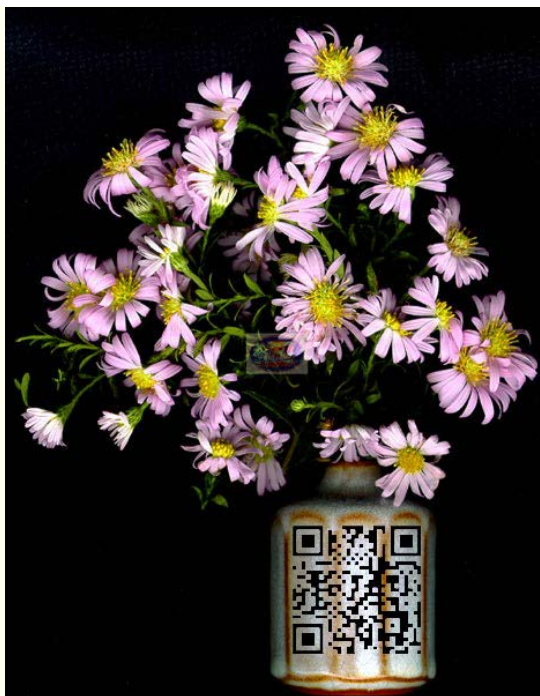


**Figure 9.** Lach, Alma. 1998. Wild Daisies. Here the QR code appears on the vase, superimposed as part of the design of the vase.  
<http://www.almalach.com/>

### Geometric Alterations beyond the Plane

#### Warping

QR codes are often presented on flat paper. That is the source of their greatest utility, currently. They also work well when displayed on a flat screen TV panel. Do they work when bent...as on the surface of an old-fashioned television screen? Inserting a QR code on the somewhat curved and bumpy surface of Google Earth might offer directions for analysis.

#### Animation

One way to go beyond layering and the limits it has in terms of successful QR code decoding, is to animate the QR code. The successive frames of the animation function as individual layers. Figure 10 illustrates a single example. While from an abstract standpoint this strategy overcomes a variety of difficulties, it is really only useful on a computer or TV screen. Thus, it might not see the same set of practical utility (except perhaps in a store window on a wide screen flat TV panel) as the static QR code does in the contemporary printed document. It is, however, an exciting prospect to consider.



Figure 10. Animation of QR codes. Do the intermediate "tweening" frames resolve correctly?

#### Layers

One way to create interesting visual effects is to layer images. The extent to which it is possible to layer images of varying opacity, shape, size, and position on an existing QR code is again a matter of balance. It is a straightforward matter, for example, to embed a QR code on the Google Earth globe. Layers of roads superimposed on the QR code might not interfere with decoding (Figure 11a). The QR code here is laid down as a mat around Buckingham Fountain in Grant Park on Chicago's beautiful lakefront. The facade of tall buildings along Michigan Avenue serves as an edge to the code.

It is tempting to want to tip the image so that the 3D buildings stand out more clearly. Doing so, however, interferes with decoding the QR code. In Figure 11b, the QR code has been elevated above many of the tall buildings to enhance its ability to be decoded--as a sort of "QR cloud."

Zooming in on the cloud (Figure 11c), from below, suggests attempting to read the QR code from underneath. Future experiments might involve aspects of flipping (reflecting) QR codes in order to do so. They might involve putting QR codes inside bubbles in Street Views or on billboards (to avoid warping inside a spherical or cylindrical bubble). In the meantime, the interested reader might work with the [attached file](#) in Google Earth.





Figure 11a. QR code covers Grant Park, Chicago Illinois. The code should scan properly.





Figure 11b. Code is adjusted so that it serves now as a cloud over the tall buildings which would otherwise interfere with proper scanning.

Institute of Mathematical Geography

Institute of Mathematical Geography

Institute of Mathematical Geography

Institute of





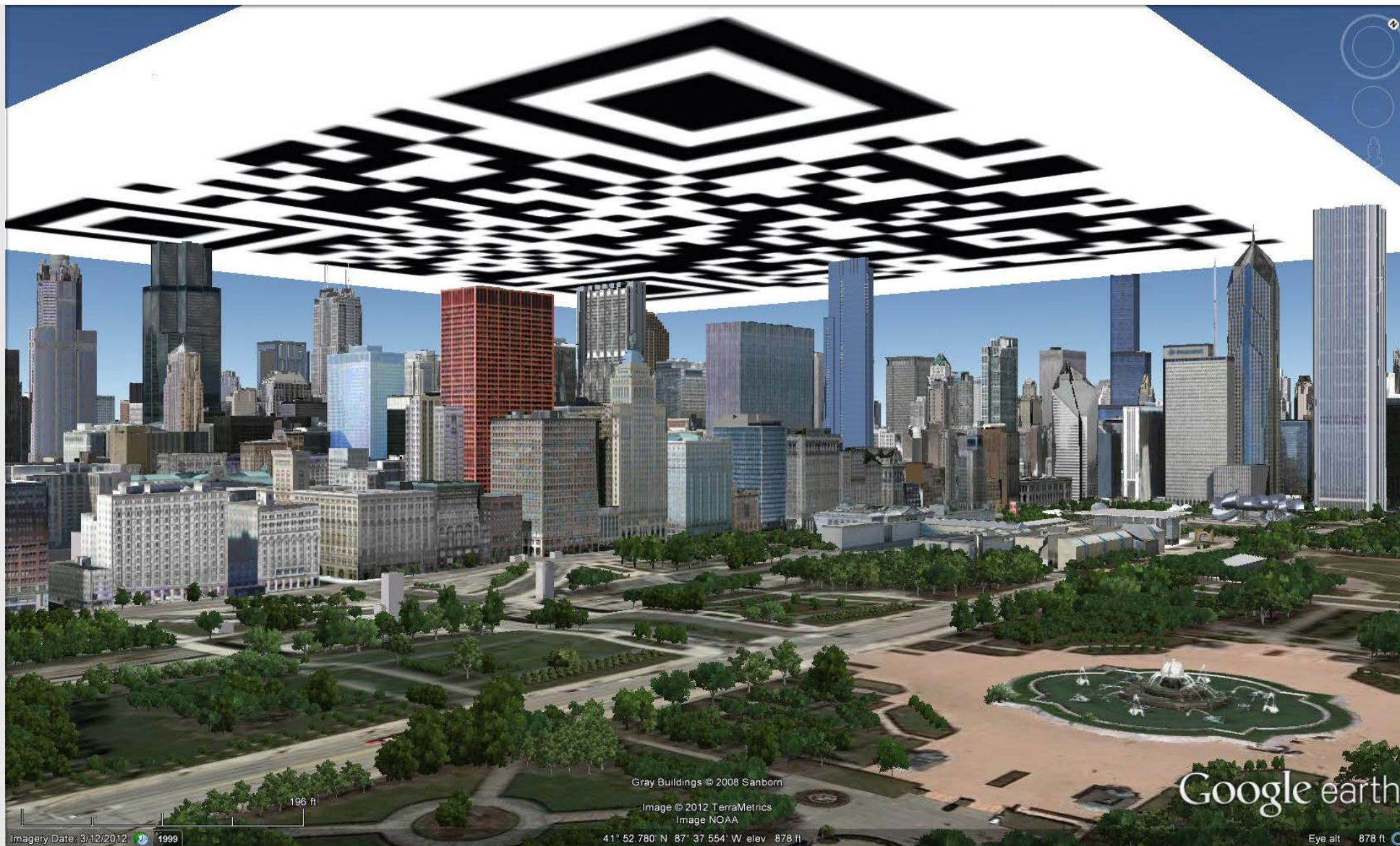


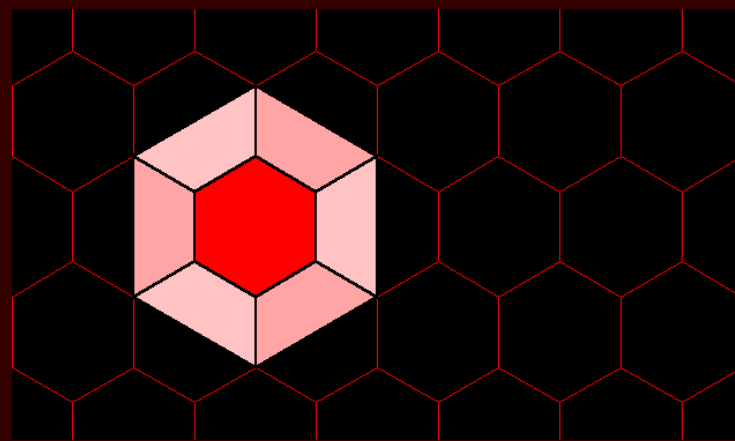
Figure 11c. Wave of the future...combine elements to create codes that scan from below...to scan the QR Cloud from the Earth!

### References

- [Beautiful Pixels](#). August 3, 2010. Last accessed Nov. 23, 2012.
- Benchoff, B. August 11, 2011. [How to put a logo in a QR code](#). Last accessed Nov. 23, 2012.
- [Google Earth](#).
- Google Search: [Color QR Code](#) Last accessed Nov. 23, 2012.
- Lach, Alma. [Pixellist Art](#). Last accessed Nov. 23, 2012.
- Pereira, I. 09/24/2012. New York is going to start putting QR codes on city permits. *AM New York*.

• **Wikipedia:**

- [A Sunday on La Grande Jatte, Georges Seurat, 1884](#). Last accessed Nov. 23, 2012.
- [Bobmath et al. 2012, February 27. QR Code Damaged](#): Last accessed, Nov. 23, 2012.
- [Goode homolosine projection](#). Last accessed Nov. 23, 2012.
- [Pointillism](#). Last accessed Nov. 23, 2012.
- [QR code](#). Last accessed, Nov. 23, 2012.



**1. ARCHIVE**

**2. Editorial Board, Advice to Authors, Mission Statement**

**3. Awards**

1.



2.



3.

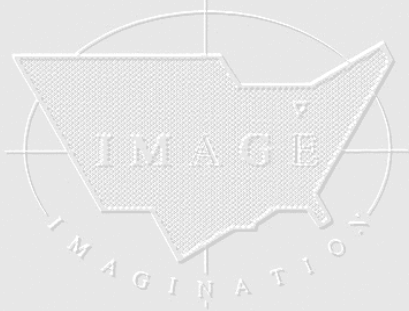




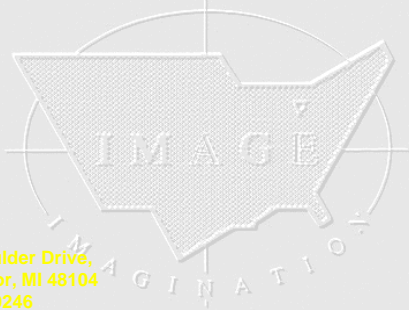
Institute of Mathematical Geography



Institute of Mathematical Geography

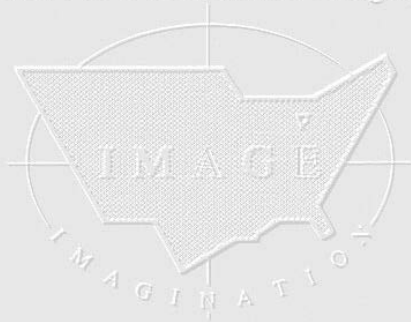


Institute of Mathematical Geography



1964 Boulder Drive,  
Ann Arbor, MI 48104  
734.975.0246  
<http://deepblue.lib.umich.edu/handle/2027.42/58219>  
[sarhaus@umich.edu](mailto:sarhaus@umich.edu)

Institute of Mathematical Geography



*Solstice: An Electronic Journal of Geography and Mathematics*,  
Institute of Mathematical Geography (IMaGe).  
All rights reserved worldwide, by IMaGe and by the authors.  
Please contact an appropriate party concerning citation of this article:  
[sarhaus@umich.edu](mailto:sarhaus@umich.edu)  
<http://www.imagenet.org>  
<http://deepblue.lib.umich.edu/handle/2027.42/58219>

*Solstice* was a **Pirelli** INTERNETional Award Semi-Finalist, 2001 (top 80 out of over 1000 entries worldwide)

One article in *Solstice* was a **Pirelli** INTERNETional Award Semi-Finalist, 2003 (Spatial Synthesis Sampler).

*Solstice* is listed in the **Directory of Open Access Journals** maintained by the University of Lund where it is maintained as a "searchable" journal.

*Solstice* is listed on the journals section of the website of the American Mathematical Society, <http://www.ams.org/>

*Solstice* is listed in **Geoscience e-Journals**

IMaGe is listed on the website of the Numerical Cartography Lab of The Ohio State University: [http://ncl.sbs.ohio-state.edu/4\\_homes.html](http://ncl.sbs.ohio-state.edu/4_homes.html)

Congratulations to all *Solstice* contributors.

Remembering those who are gone now but who contributed in various ways to *Solstice* or to IMaGe projects, directly or indirectly, during the first 25 years of IMaGe:

**Allen K. Philbrick | Donald F. Lach | Frank Harary | William D. Drake | H. S. M. Coxeter | Saunders Mac Lane | Chauncy D. Harris | Norton S. Ginsburg | Sylvia L. Thrupp | Arthur L. Loeb | George Kish |**

# SOLSTICE:

## An Electronic Journal of Geography and Mathematics

Persistent URL:

<http://deepblue.lib.umich.edu/handle/2027.42/58219>



Deep Blue



IMaGe Home



Solstice Home



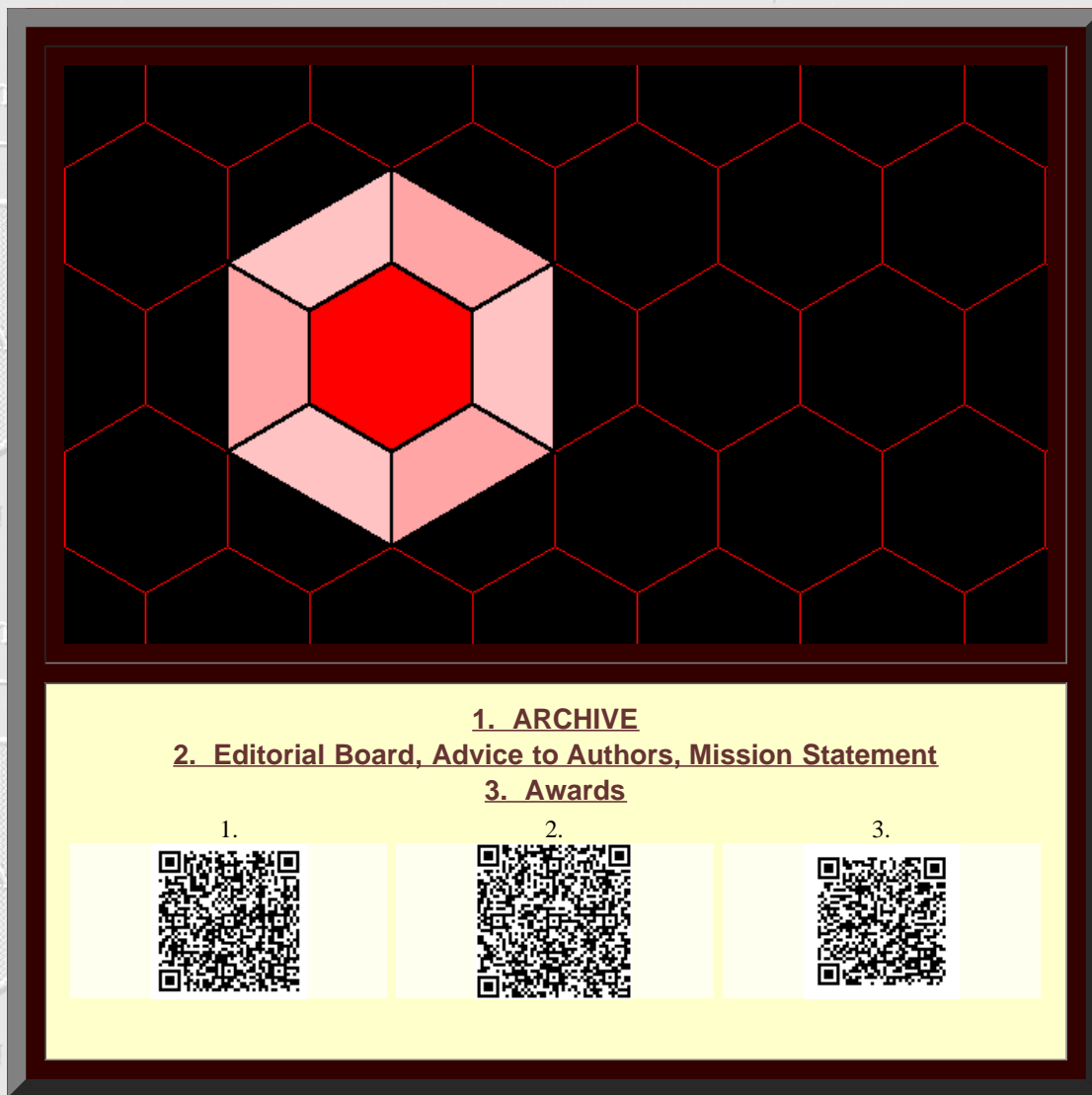
Institute of Mathematical Geography, All rights reserved in all formats.

Works best with a high speed internet connection.

Final version of IMAge logo created by Allen K. Philbrick from original artwork from the Founder.

- **William C. Arlinghaus** shared this link on creating mathematical notation: <http://gadgetwise.blogs.nytimes.com/2012/08/03/tip-of-the-week-doing-math-in-windows-7/>
- **David Gitterman** shared this link on "Sandy's Island." <http://www.tgdaily.com/general-science-brief/67686-island-undiscovered-by-scientists#.ULNV2g6YJJs.email>
- **Karen Hart** wrote to share this link to Mark Newman's cartograms of election results: <http://www-personal.umich.edu/~mejn/election/2012/>
- **Harold Moellering** wrote to share this link on the Hilbert Curve map as possible motivation for other applications of its content: <http://www.dcwg.org/new-hilbert-curve-maps-of-the-infections/>
- **From Joseph Kerski:** I created 2 StoryMaps (first two links below) in part so I could help others generate these and I thought you might be interested in the first one in particular. They have great potential for education.
  - **Lost Detroit:** <http://www.josephkerski.com/storymaps/lostdetroit/>
  - **20 on 40: 20 Stops along 40 Degrees North Latitude--**<http://www.josephkerski.com/storymaps/40north/>
  - **More generally, link to the main storymaps page:** <http://storymaps.esri.com> This link is where people can access the templates and create their own storymaps (as well as browse the 100 or so that have


already been created on a wide variety of topics).





**1. ARCHIVE**

**2. Editorial Board, Advice to Authors, Mission Statement**

**3. Awards**

1. 

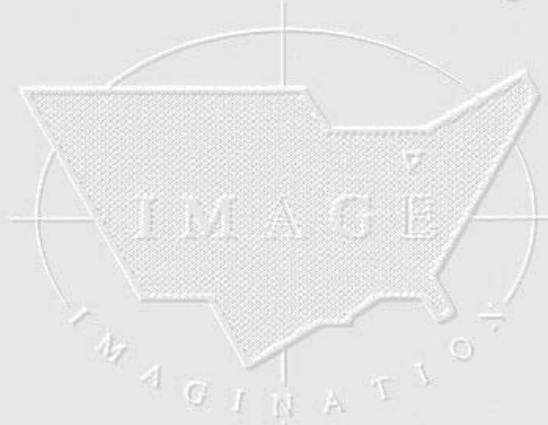
2. 

3. 





## Institute of Mathematical Geography



*Solstice: An Electronic Journal of Geography and Mathematics*,  
Institute of Mathematical Geography (IMaGe).

All rights reserved worldwide, by IMaGe and by the authors.  
Please contact an appropriate party concerning citation of this article:

[sarhaus@umich.edu](mailto:sarhaus@umich.edu)

<http://www.imagenet.org>

<http://deepblue.lib.umich.edu/handle/2027.42/58219>

*Solstice* was a **Pirelli** INTERNETional Award Semi-Finalist, 2001 (top 80 out of over 1000 entries worldwide)

One article in *Solstice* was a **Pirelli** INTERNETional Award Semi-Finalist, 2003 (Spatial Synthesis Sampler).

*Solstice* is listed in the [Directory of Open Access Journals](#) maintained by the University of Lund where it is maintained as a "searchable" journal.

*Solstice* is listed on the journals section of the website of the American Mathematical Society, <http://www.ams.org/>

*Solstice* is listed in [Geoscience e-Journals](#)

IMaGe is listed on the website of the Numerical Cartography Lab of The Ohio State University: [http://ncl.sbs.ohio-state.edu/4\\_homes.html](http://ncl.sbs.ohio-state.edu/4_homes.html)

---

Congratulations to all *Solstice* contributors.

Remembering those who are gone now but who contributed in various ways to *Solstice* or to IMaGe projects, directly or indirectly,

Institute of Mathematic

during the first 25 years of IMAge:

Allen K. Philbrick | Donald F. Lach | Frank Harary | William D. Drake |  
H. S. M. Coxeter | Saunders Mac Lane | Chauncy D. Harris | Norton S.  
Ginsburg | Sylvia L. Thrupp | Arthur L. Loeb | George Kish |

aphy

Institute of Math

1964 Boulder Drive,  
Ann Arbor, MI 48104  
734.975.0246

<http://deepblue.lib.umich.edu/handle/2027.42/58219>  
[sarhaus@umich.edu](mailto:sarhaus@umich.edu)